

Measurements of OH and HO₂ concentrations during the MCMA-2006 field campaign – Part 2: Model comparison and radical budget

S. Dusanter¹, D. Vimal^{1,*}, P. S. Stevens¹, R. Volkamer², L. T. Molina^{3,4}, A. Baker⁵, S. Meinardi⁵, D. Blake⁵, P. Sheehy^{3,4}, A. Merten^{6,**}, R. Zhang⁷, J. Zheng⁷, E. C. Fortner^{8,***}, W. Junkermann⁹, M. Dubey¹⁰, T. Rahn¹⁰, B. Eichinger¹¹, P. Lewandowski¹¹, J. Prueger¹², and H. Holder¹³

¹Center for Research in Environmental Science, School of Public and Environmental Affairs, and Department of Chemistry, Indiana University, Bloomington, IN 47405, USA

²Department of Chemistry and Biochemistry, University of Colorado, USA

³Molina Center for Energy and the Environment USA

⁴Department of Earth, Atmospheric, and Planetary Sciences, Massachusetts Institute of Technology, USA

⁵University of California, Irvine, 92697 CA, USA

⁶Institute of Environmental Physics, University of Heidelberg, Germany

⁷Department of Atmospheric Sciences, Texas A&M University, USA

⁸Department of Chemistry, Montana State University, USA

⁹Forschungszentrum Karlsruhe, Institute of Meteorology and Climate Research, IMK-IFU, Garmisch-Partenkirchen, Germany

¹⁰Earth and Environmental Sciences Division, Los Alamos National Laboratory, USA

¹¹IIHR-Hydroscience & Engineering, University of Iowa, Iowa City, IA, USA

¹²USDA National Soil Tilth Lab, Ames, IA, USA

¹³Duke University, Durham, NC, USA

* now at: SRI International, Menlo Park, CA, USA

** now at: Institute of Applied Photophysics, Dresden University of Technology, Germany

*** now at: Aerodyne Research Incorporated, 45 Manning Road, Billerica, MA, USA

Received: 20 March 2009 – Published in Atmos. Chem. Phys. Discuss.: 17 April 2009

Revised: 10 August 2009 – Accepted: 10 August 2009 – Published: 15 September 2009

Abstract. Measurements of hydroxyl (OH) and hydroperoxy (HO₂) radicals were made during the Mexico City Metropolitan Area (MCMA) field campaign as part of the MILAGRO (Megacity Initiative: Local and Global Research Observations) project during March 2006. These measurements provide a unique opportunity to test current models of atmospheric RO_x (OH + HO₂ + RO₂) photochemistry under polluted conditions. A zero-dimensional box model based on the Regional Atmospheric Chemical Mechanism (RACM) was constrained by 10-min averages of 24 *J*-values and the concentrations of 97 chemical species. Several issues related to the RO_x chemistry under polluted conditions

are highlighted in this study: (i) Measured concentrations of both OH and HO₂ were underpredicted during morning hours on a median campaign basis, suggesting a significant source of radicals is missing from current atmospheric models under polluted conditions, consistent with previous urban field campaigns. (ii) The model-predicted HO₂/OH ratios underestimate the measurements for NO mixing ratios higher than 5 ppb, also consistent with previous urban field campaigns. This suggests that under high NO_x conditions, the HO₂ to OH propagation rate may be overestimated by the model or a process converting OH into HO₂ may be missing from the chemical mechanism. On a daily basis (08:40 a.m.–06:40 p.m.), an analysis of the radical budget indicates that HONO photolysis, HCHO photolysis, O₃-alkene reactions and dicarbonyls photolysis are the main radical sources. O₃



Correspondence to: S. Dusanter
(sdsante@indiana.edu)

photolysis contributes to less than 6% of the total radical production.

1 Introduction

Understanding the photochemical production of O₃ and secondary organic aerosols (SOA), as well as their sensitivity to emissions of volatile organic compounds (VOCs) and nitrogen oxides (NO_x = NO + NO₂) is crucial to the design of air quality control strategies. For instance, to prevent the formation of O₃ over urban and rural areas, traditional approaches rely on reducing VOCs emissions under the NO_x-saturated regime, or nitrogen oxides emissions under the NO_x-limited regime (Sillman, 1993, 1999). However, the NO_x concentration threshold characterizing the transition between NO_x-saturated and NO_x-limited regimes is not easy to identify due to the wide range of VOCs encountered in the atmosphere. In addition, the O₃ production sensitivity likely changes with photochemical aging as the air mass travels away from emission sources (i.e. an air mass can be NO_x-saturated over urban areas and NO_x-limited downwind) (Sillman, 1993). Strategies efficient at the local urban scale are likely to be inefficient at the regional scale, and this limits the reliability of such controls to prevent O₃ formation.

To establish efficient control strategies, a detailed understanding of the free radical budget is essential since production of O₃ and other secondary pollutants is limited by the pool of radicals available to initiate the oxidation of the primary VOCs. Several studies focusing on RO_x (OH + HO₂ + RO₂) chemistry under urban conditions are reviewed in a companion paper (Dusanter et al., 2009) as well as in the literature (Kanaya et al., 2007; Sheehy et al., 2008). Recently, there have been several detailed studies focused on the radical budget in urban areas, including the 2003 Mexico City Metropolitan Area field campaign (Volkamer et al., 2007b), the 2003 Tropospheric ORganic Chemistry experiment (TORCH) (Emmerson et al., 2007) and the 1999–2000 Pollution of the Urban Midlands Atmosphere (PUMA) field campaign (Emmerson et al., 2005b). These studies highlight the complex nature of urban environments where OH production is not dominated by O₃ photolysis and additional sources of RO_x radicals are important contributors to the radical initiation (Emmerson et al., 2005b; Volkamer et al., 2007b). A good example is nitrous acid (HONO) whose photolysis occurs at longer wavelengths than O₃ photolysis and thus can be an important source of OH both in the early morning (Holland et al., 2003) and during the day (Ren et al., 2003; Kleffmann, 2007). Note that in urban environments, photolysis of secondary oxygenated species and O₃-alkene reactions can also contribute significantly to the total RO_x initiation (Emmerson et al., 2005b).

The photochemistry of urban environments is characterized by a complex coupling between initiation, termination

and propagation of RO_x radicals that leads to the cycling of OH through RO₂ and HO₂. For example, the OH-initiated oxidation of VOCs leads to the loss of OH and the production of peroxy radicals (RO₂). Under low NO_x conditions, the cross-reactions involving RO₂ and HO₂ will lead to termination of the radicals through the formation of peroxides and other species. However, under moderate and high levels of NO_x (a few ppb to hundreds of ppb) usually observed in urban and suburban environments, the RO₂ radicals will be propagated to HO₂ and then to OH through successive reactions involving NO. OH is regenerated and can oxidize more VOCs. This efficient radical cycling leads to a catalytic oxidation of the primary VOCs and a fast production of O₃ and secondary oxygenated species, with some of the latter acting as additional HO_x sources.

Understanding the complex radical chemistry of the atmosphere requires the use of a chemical mechanism that can reproduce RO_x chemistry. Several mechanisms have been developed, tested against atmospheric chamber data, and used to investigate and predict atmospheric concentrations of important chemical species during field experiments. The Master Chemical Mechanism (MCM) and the Regional Atmospheric Chemical Mechanism (RACM) are among the most widely used mechanisms in atmospheric chemistry. MCM is an explicit mechanism developed at the University of Leeds (Jenkin et al., 1997, 2003; Saunders et al., 2003) that contains the detailed degradation of 135 VOCs using more than 13 500 chemical reactions. In contrast, RACM is a condensed mechanism (Stockwell et al., 1997), which relies on lumping techniques to reduce the number of reactions to 237, and as a result is less demanding in terms of computing time. MCM and RACM have been widely used over the last decade to test the ability of current atmospheric chemical mechanisms to reproduce the RO_x chemistry under various types of environments (remote, forested, urbanized) (Heard and Pilling, 2003).

This manuscript presents a modeling effort performed to test our understanding of the daytime RO_x photochemistry over highly polluted areas such as megacities. The Mexico City Metropolitan Area (MCMA) field campaign at the T0 supersite (Instituto Mexicano del Petroleo) during March 2006 was characterized by measured concentrations of VOCs and NO_x that were higher than other previous field campaigns and represents a unique dataset to assess the RO_x photochemistry in a polluted environment. A zero-dimensional box model, including chemistry based on the Regional Atmospheric Chemical Mechanism (RACM), was used to predict the concentrations of OH, HO₂, RO₂ radicals and their rates of initiation, propagation and termination. The primary goal of this paper is threefold: (i) Compare predicted and measured HO_x concentrations using both daily concentration profiles and campaign median profiles. (ii) Investigate the key reactions driving initiation, termination and cycling of the RO_x radicals to assess the radical budget. (iii) Compare the conclusions achieved for MCMA-2006 using a

model based on the RACM mechanism to that observed for MCMA-2003 using both RACM (Shirley et al., 2006) and MCM (Sheehy et al., 2008).

2 Instrumentation deployed at T0 during MCMA-2006

Meteorological parameters, photolysis frequencies and concentrations of chemicals were measured at the Instituto Mexicano del Petroleo (supersite T0) during March 2006. Chemical species pertinent for this study are displayed in Table 1 and 2 together with uncertainties and detection limits. All the instruments were located on the roof of building 32.

Diurnal concentrations of OH and HO₂ were measured by Laser-Induced Fluorescence, using the Indiana University Fluorescence Assay by Gas Expansion instrument (IU-FAGE). These measurements took place from 14 to 31 March. The deployment of IU-FAGE and the HO_x concentrations measured during MCMA-2006 are presented in a companion paper (Dusanter et al., 2009). Briefly, ambient air is expanded into a low pressure cell where OH is excited by a laser beam, whose wavelength is adjusted on-resonance with an OH absorption line. The resulting fluorescence is collected and quantified by a gated detection system whose sensitivity was calibrated using two different approaches to generate a known concentration of OH; the production of a steady state concentration of OH from O₃-alkene reactions and the production of OH from photolysis of water-vapor at 185-nm (Dusanter et al., 2008). Concentrations of HO₂ were measured indirectly, after chemical conversion into OH by addition of nitric oxide in the sampling cell.

A Proton Transfer Reaction-Mass Spectrometry (PTR-MS) instrument from Texas & AM University measured the concentrations of several VOCs (Table 1) on 5–23 March and 26–31 March. Calibration and background check procedures are described in Fortner et al. (2009). Two LP-DOAS (Long-Path Differential Optical Absorption Spectroscopy) instruments were deployed at T0. Concentrations of aromatic species (benzene, toluene, xylenes, ethylbenzene, benzaldehyde, styrene) were measured by a first DOAS telescope coupled with two reflector arrays (DOAS1, 2052-m and 440-m back and forth). A second DOAS telescope (DOAS2) was employed to monitor concentrations of O₃, NO₂, HCHO, HONO, SO₂ and glyoxal on a pathlength of 5285-m (back and forth), opposite to the first DOAS telescope. The two LP-DOAS instruments were previously deployed during MCMA-2003 and additional information are available elsewhere (Volkamer et al., 2007b). In addition to LP-DOAS measurements, local point formaldehyde concentrations were monitored using an instrument based on the Hantzsch chemistry fluorimetric detection of formaldehyde in liquid phase (Junkermann and Burger, 2006). Whole air canister samples were also collected at T0 (59 samples) and the Universidad Tecnológica de Tecamac (T1, 202 samples) in stainless steel canisters. Samples were collected over peri-

ods of 30–60 min at T0 and analyzed using chromatographic analysis. The measurements covered 22 alkanes, 11 alkenes, 14 aromatic species along with CO, ethyne, isoprene and alpha and beta-pinene. The 1σ precision ranged from 0.5 to 12% for alkanes, 11 to 34% for alkenes and 2 to 10% for aromatic species (Colman et al., 2001). Measurements of O₃ (Teledyne 400E) and NO_x (Thermo Environmental) were performed using commercial monitors based on UV absorption spectroscopy and chemiluminescence of NO₂.

Photolysis frequencies for NO₂→NO+O(³P), O₃→O(¹D)+O₂, HONO→HO+NO, HCHO→H+HCO and HCHO→H₂+CO were directly measured using a spectroradiometer as described for MCMA-2003 (Volkamer et al., 2007b). Uncertainties are estimated to be 25% for *J*(O¹D) and 15% for *J*(NO₂), *J*(HONO) and *J*(HCHO).

3 Modeling procedures

This study relies on a zero-dimensional box model based on the Regional Atmospheric Chemical Mechanism (RACM) (Stockwell et al., 1997). RACM is a condensed chemical mechanism which describes the gas-phase oxidation of 17 inorganic and 32 organic species. Only 9 organic species are treated explicitly and 23 are surrogates that group several chemical species based on their emission rates, chemical structure and reactivity with OH.

Kinetic parameters for the reactions of OH, O₃ and NO₃ with inorganic species were updated using the JPL database (Sander et al., 2006). Note that the chemical reaction between OH and NO₂ is the main sink for odd hydrogen radicals under polluted conditions. Recent investigations have shown that in addition to the formation of nitric acid (HONO₂), a second pathway leads to the formation of a weakly bound adduct (peroxynitrous acid, HOONO) whose thermal decomposition quickly reproduces OH and NO₂. Neglecting this second channel would lead to an overestimation of the radical sinks by approximately 10–15% and thus an underprediction of the radical concentrations. For this study the rate constant of NO₂+OH→HONO₂ was taken as that recommended by Sander et al. (2006).

Kinetic parameters for reactions involving organic species treated explicitly in RACM (methane, ethane, ethene, formaldehyde, glyoxal, methyl peroxide and isoprene) were also updated using the JPL database. Kinetic rate constants and branching ratios for OH, O₃ and NO₃ reactions with surrogate species (HC3, HC5, HC8, OLT, OLI, DIEN, TOL, XYL, CSL, ALD, KET, API, MGLY, DCB, UDD, HKET, ONIT, PAN, TPAN, OP2, PAA, ORA1, ORA2) were used as described for RACM (Stockwell et al., 1997). Heterogeneous chemistry, such as the incorporation of trace gases into aerosols, was not included in the model.

The model was constrained by 10-min average measurements of temperature, pressure, *j*-values (Table S1, supplementary material <http://www.atmos-chem-phys.net/9/6655/>

Table 1. ^a Average value are displayed for species treated explicitly in RACM and are calculated using the median campaign measurements (14–22 and 27–28 March) from 08:40 a.m. to 06:40 p.m. ^b In unit of 10⁶ cm⁻³. ^c HO₂ was measured for 15-s every 8–15 min. ^d Integrated measurement time. Shaded areas indicate the measurements used to constrain RACM.

Species	Time resolution (min)/Uncertainty (%)/ detection limit (ppb)	Instrumentation	Institution	Reference	Mixing ratio ^a (ppb)
Radical Species					
OH	7.5–30/20/0.7–3.3 ^b	LIF-FAGE	Indiana University	(Dusanter et al., 2008a)	3.2 ^b
HO ₂	8–15 ^c /21/4.4–28.0 ^b	LIF-FAGE	Indiana University	(Dusanter et al., 2008a)	126.0 ^b
Inorganic Species					
O ₃	10/10/0.1 ~7/5/3.2	UV absorption LP-DOAS (DOAS2)	Indiana University MIT, U. of Heidelberg	(Dusanter et al., 2008a)	56.2
NO	10/10/0.1	Chemiluminescence	RAMA	(Dusanter et al., 2008a)	16.4
NO ₂	10/10/0.1 ~5/5/0.5 ~3/5/0.4	Chemiluminescence LP-DOAS (DOAS2)	RAMA MIT, U. of Heidelberg	(Dusanter et al., 2008a) (Merten, 2008)	28.4
HONO	~5/5/0.01	LP-DOAS (DOAS1)	MIT, U. of Heidelberg	(Merten, 2008)	0.43
SO ₂	~5/5/0.02	LP-DOAS (DOAS2)	MIT, U. of Heidelberg	(Merten, 2008)	3.4
CO		LP-DOAS (DOAS2)	Earth and Environmental Sciences, LANL		765
H ₂			Earth and Environmental Sciences, LANL		679
H ₂ O			U. of Iowa, Duke U., National Soil Tilth Lab.		0.66%
Organic Species					
Methanol, ethanol, acetonitrile, acetaldehyde Benzene, C3-benzene, ethylacetate Toluene, C2-benzene, styrene, isoprene, monoterpenes, DMS, acetone + propanal formaldehyde	1.3/39/– 1.3/30/– 1.3/26/– 2/12/0.2	PTRMS Hantzsch liquid phase fluorimetric detection	Department of Atmospheric Sciences, Texas A&M University Institute of Meteorology and Climate Research, Forschungszentrum	(Fortner et al., 2008)	8.9
glyoxal	~5/5/0.40	LP-DOAS (DOAS2)	MIT, U. of Heidelberg	(Merten, 2008)	
Benzaldehyde	~5/5/0.20 ~5/5/0.13	LP-DOAS (DOAS2) LP-DOAS (DOAS1)	MIT, U. of Heidelberg U. of Heidelberg	(Merten, 2008) (Merten, 2008)	0.45
VOCs speciation	30–60 ^d /0.5–34/0.005	Canister sampling/ Gas Chromatography	U. of California		

2009/acp-9-6655-2009-supplement.pdf), inorganic species (Table 1) and organic species (Tables 1 and 2). Table 2 displays an exhaustive list of all the organic species treated explicitly and grouped in each surrogate for this study. The differential equation system generated from the chemical mechanism was integrated by the FACSIMILE solver using an integration time of 30 h for each 10-min data points. This approach insures that all the species affecting the RO_x chemistry have reached a steady-state balance. During the 30-h integration period, the constrained parameters were reinitialized to their initial values every ten seconds.

A total of 24 photolysis frequencies are required to constrain the model (Table S1, supplementary material <http://www.atmos-chem-phys.net/9/6655/2009/acp-9-6655-2009-supplement.pdf>). Unmeasured *J*-values were calculated as a function of solar zenith angle at the coordinates of T0 (latitude 19.48872°, longitude –99.14729°) using the Master Chemical Mechanism (MCM) parameterization (Jenkin et al., 1997; Saunders et al., 2003). This parameterization relies on the calculation of *J*-values for clear sky conditions, an O₃ column density of 345 Dobson units and an altitude of 0.5 km. Calculated *J*-values were corrected for the effect of altitude, clouds, aerosols and O₃ column density using two different scaling factors. For

chemical species photolyzed at wavelengths shorter than 330-nm, the scaling factor was derived from the ratio between measured and calculated *J*(O¹D) values. For species photolyzed at wavelengths longer than 330-nm, measured and calculated *J*(NO₂) values were used instead of *J*(O¹D). Note that HONO and HCHO absorb in the same wavelength range as NO₂ and O₃ respectively, and using *J*(HONO) and *J*(HCHO→H+HCO) lead to similar correction factors as using *J*(NO₂) and *J*(O¹D). The correction factor derived from *J*(O¹D) was usually 20–30% different than that from *J*(NO₂) between 10:00 a.m. and 02:00 p.m. (CST), as photolytic processes occurring at short wavelengths are likely to exhibit a greater dependence on the O₃ column density. This point highlights the recommendations of Monks et al. (2004) to be careful when scaling unmeasured photolysis frequencies during field measurements.

As an additional check, *J*-values were also calculated using the Tropospheric Ultraviolet-Visible (TUV 4.4) model (Madronich, 1989; Madronich and Weller, 1990), and were corrected using the scaling procedure described above. Corrected *J*-values from the MCM parameterization and from TUV agree to within 5–20%. Finally the corrected photolysis frequencies were multiplied by a factor of 1.04 to account for surface albedo when sampling the HO_x radicals at 1-m above

Table 2.^a Average value calculated using the median campaign (14–22 and 27–28 March) between 08:40 a.m. and 06:40 p.m. SF: Scaling Factor.

Surrogate	Species included	Method of calculation	Fraction ^a	Mixing ratio ^a
CH ₄	CH ₄	Canister speciation vs. Toluene	100%	2.3 ppm
ETH	Ethane	Canister speciation vs. Toluene	100%	6.2 ppb
ETE	Ethene	Canister speciation vs. Toluene	100%	6.9 ppb
ISO	Isoprene	Measured	100%	0.32 ppb
API	Monoterpenes	Measured	100%	0.14 ppb
HC3	Methanol, ethanol, acetonitrile, ethylacetate	Measured	>99%	78.9 ppb
	Propane, i-butane, n-butane, 2,2-dimethylbutane, ethyne	Canister speciation vs. Toluene		
	n-propylacetate, i-propylacetate, Methyl t-butyl ether	SF/benzene (Sheehy et al., 2008)	<1%	
HC5	i-pentane, n-pentane, n-hexane, 2-methyl pentane, 3-methyl pentane, 2,2,4-trimethyl pentane, 2,3,4-trimethyl pentane, Cyclopentane	Canister speciation vs. Toluene	93%	12.7 ppb
	n-butyl acetate	SF/benzene (Sheehy et al., 2008)	7%	
	1-propanol, 2-propanol	SF/methanol (Sheehy et al., 2008)		
HC8	DMS	Measured	24%	13.2 ppb
	n-heptane, n-octane, n-nonane, n-decane, 2,4-dimethylpentane, methylcyclopentane, cyclohexane	Canister speciation vs. Toluene		
	3-methylhexane, 2-methylhexane, i-octane, 2,3-dimethylbutane, 2,3-dimethylpentane, methylcyclohexane, 2,4-dimethyl hexane, 2,5-dimethylhexane, methyl heptane	SF (Velasco et al., 2007)	26%	
	1-butanol, 2-butanol, 2-methyl-1-pentanol, 2-methyl-2-pentanol, 2-methoxyethanol, 2-ethoxyethanol, 1-methoxy-2-propanol, 2-butoxyethanol, 1-butoxy-2-propanol, ethylene glycol, propylene glycol	SF/methanol (Sheehy et al., 2008)	50%	
OLT	Propene, 1-butene, i-butene, 3-methyl-1-butene	Canister speciation vs. Toluene	92%	3.0 ppb
	2-methyl-1-butene, 1-hexene	SF (Velasco et al., 2007)	8%	
OLI	Trans-2-butene, cis-2-butene, trans-2-pentene, cis-2-pentene, 2-methyl-2-butene	Canister speciation vs. Toluene	100%	0.80 ppb
TOL	Toluene, benzene	Measured		8.5 ppb
	i-propylbenzene, n-propylbenzene,	Canister speciation vs. C3-benzene	100%	
	Ethylbenzene	Canister speciation vs. C2-benzene		
XYL	Styrene	Measured		4.3 ppb
	Sum xylenes	Canister speciation vs. C2-benzene	100%	
	Sum trimethylbenzenes	Canister speciation vs. C3-benzene		
	Sum ethyltoluenes	Canister speciation vs. C3-benzene		
ALD	Acetaldehyde, benzaldehyde	Measured	90%	5.0 ppb
	Propanal	SF/HCHO (Sheehy et al., 2008)	10%	
GLY	Glyoxal	Measured	100%	0.42 ppb
DIEN	Butadiene	Canister speciation vs. Toluene	100%	0.09 ppb
KET	Acetone	Measured	100%	10.2 ppb

the roof of the building. Note that collocated measurements of the downward flux were not performed during MCMA-2006. However, surfaces usually exhibit albedos of 2–10% and the factor 1.04 is a rough estimate for a dark brown roof. For comparison, Sheehy et al. (2008) used a factor 1.08 to correct for surface albedo when the HO_x instrument was located on a small tower (6 m) on the roof of the CENICA building in Mexico City. Given that two scaling factors were used to estimate unmeasured *J*-values in this study, we estimate that the uncertainty on the calculated *J*-values is only 10% higher than that observed for the measured *J*-values. Note that measured *J*-values were missing for 14 March and the morning of 15 March so calculated *J*-values for these days were used without correction.

A non-exhaustive list of organic and inorganic chemical species measured at T0 is displayed in Table 1. Concentrations were averaged or interpolated on 10-min intervals depending on the measurement time resolution. Missing measurements were linearly interpolated when the gap was less than 3 h.

NO₂ concentrations were measured using a commercial chemiluminescence/Mb catalyst monitor collocated to IU-FAGE and two LP-DOAS instruments (DOAS1 and DOAS2). Local point concentrations of NO₂ measured by chemiluminescence would be more suitable for radical modeling since OH and HO₂ were measured locally. However, such instruments are prone to interferences in urban environments, where high concentrations of nitric acid and alkyl nitrates can lead to artificially enhanced NO₂ measurements (Dunlea et al., 2007). A comparison of 10-min time-resolved concentrations of NO₂ using median campaign measurements indicated that the concentrations measured by chemiluminescence were systematically higher by a factor of approximately 1.4 than those measured by LP-DOAS. As a consequence, our model was constrained to the LP-DOAS measurements of NO₂.

Table 2 displays the VOCs used to constrain the model. Air canister sampling was performed from 6 to 31 March at various sites in Mexico City with an integrated measurement time of approximately 30–60 min (T0) and 3 h (T1),

including 4 days of measurements at T0 (16, 19, 28, and 30 March). Linear functions of each non-aromatic VOC with toluene were derived from the canister measurements to estimate time-resolved VOC concentrations for the days of modeling. This analysis was performed for the full set of VOCs measured at T0 and T1 and the VOCs measured at T0 only. Both analyses led to similar linear functions for each individual VOC, with correlation coefficients in the range of 0.80–0.91 (37 VOCs), except for methane, n-hexane, 1-pentene, 3-methyl-1-butene, trans-2-butene, cis-2-butene, trans-2-pentene, cis-2-pentene and 2-methyl-2-butene whose correlation coefficients were in the range 0.52–0.67. The good correlation coefficients suggest a short photochemical aging of the urban air masses due to active venting in the MCMA (De Foy et al., 2006) and fresh emissions throughout the day. The linear functions were used to estimate 10-min time-resolved VOC concentrations using toluene concentrations measured by PTRMS. Toluene was chosen instead of CO and benzene because measurements of toluene from three different techniques (canister sampling/GC FID, DOAS and PTRMS) were in very good agreement at T0. 10-min time-resolved concentrations of aromatic compounds such as *i*- and *n*-propylbenzene, trimethylbenzenes, ethylbenzenes, ethyltoluenes and xylenes were estimated using the speciation observed in canister sampling and scaled to the measured C2- and C3-benzene from PTRMS.

There is evidence that a large fraction of VOCs are usually not measured during field campaigns (Lewis et al., 2000; Velasco et al., 2007; Elshorbany et al., 2009). For completeness of the VOC libraries used in this study, concentrations of unmeasured VOCs were estimated using scaling factors derived for the MCMA-2003 field campaign (Sheehy et al., 2008). Additional scaling factors were calculated for unmeasured VOCs using a procedure based on averaged ambient concentrations reported for MCMA-2003 (Velasco et al., 2007) from several urban sites (Table 4 in Velasco et al., 2007). For instance, while 3-methyl hexane (3MH) was measured in 2003, no ambient concentrations were reported for 2006. The bimolecular rate constant for OH + 3MH (7.20×10^{-12} cm³/molecule/s, 298 K, 1 atm) is similar to that recommended for *n*-heptane (7.15×10^{-12} cm³/molecule/s, 298 K, 1 atm), which was measured during both campaigns. The concentration ratio 3MH/*n*-heptane observed during 2003 was used to estimate ambient concentrations of 3MH for 2006 using measured concentrations of *n*-heptane. Different reference compounds were used to estimate ambient concentrations of other chemical species for 2006, providing that the rate constant with OH was similar for both compounds. This methodology assumes a similar speciation of VOCs in 2003 and 2006 and also assumes that the scaling factors are constant throughout the day. The latter point is supported by the good correlations found between VOCs in air canister measurements for MCMA-2006. In addition, Shirley et al. (2006) observed constant ratios between VOCs throughout the day for MCMA-2003. Ta-

ble 2 displays the contribution of estimated VOCs to the total amount of VOCs included in each RACM surrogate. While this contribution is considerable for HC8 (76%) and significant for ALD (10%) and OLT (8%), the total OH reactivity increases by only 7.8% on a median campaign basis. Concentrations of unconstrained species and rates of radical fluxes (i.e. initiation, termination and propagation of RO_x radicals) were directly calculated by the model. The subset of chemical reactions that were selected to calculate the rates of radical fluxes are presented in the supplementary material as Table S2 <http://www.atmos-chem-phys.net/9/6655/2009/acp-9-6655-2009-supplement.pdf>.

While measurements of OH reactivity performed during the MCMA-2003 field campaign appears to be consistent to within 30% with that calculated from the measured pool of VOCs and NO_x (Shirley et al., 2006), such measurements were not performed during MCMA 2006. Potential missing OH reactivity, observed in some environments (Kovacs et al., 2003; Di Carlo et al., 2004; Yoshino et al., 2006; Sinha et al., 2008), cannot be ruled out for the T0 site. It should be noted that measuring the total loss rate of OH during field campaigns is a valuable and important addition to the pool of measurements usually performed to understand atmospheric photochemistry.

Uncertainty on the calculated concentrations of OH and HO₂ were investigated by Shirley et al. (2006) for RACM under comparable polluted conditions during MCMA-2003. A Monte Carlo approach led to 2σ uncertainties of $\pm 45\%$ for OH and $\pm 70\%$ for HO₂. Analogous uncertainties on the constrained quantities and the kinetic parameters used in this study are likely to lead to comparable uncertainties on the calculated HO_x concentrations and we assume uncertainty factors of 1.5 and 1.7 for the predicted OH and HO₂ respectively. It is worth noting that a sensitivity analysis performed for this study by varying the concentrations of several constrained species is consistent with the errors on modeled OH and HO₂ concentrations stated above (Table S6, supplementary material <http://www.atmos-chem-phys.net/9/6655/2009/acp-9-6655-2009-supplement.pdf>).

Ancillary measurements overlapped with measured HO_x concentrations on 14–22 and 27–28 March and libraries of constrained parameters were built for these 11 days. Several base cases were selected to test the model predictions. (i) Libraries of chemical species containing only the measured VOCs (called “short VOCs set”) and (ii) libraries containing additional estimated VOCs (called “large VOCs set”, see above) were used to perform modeling for individual days. (iii) Median and averaged concentration profiles of the constrained species, calculated for the 11 days of modeling and matching the availability of the measured HO_x concentrations, were also used to predict median and averaged campaign RO_x concentrations.

4 Results/Discussion

Section 4.1 addresses uncertainties associated with constraining RACM for this study using measured and predicted concentrations of long-lived chemical species such as HONO, NO₂ and glyoxal. Section 4.2 highlights the model sensitivity to input parameters. HO_x concentrations were simulated by varying the model inputs (HC3 + HC5 + HC8, OLT + OLI, KET, CO, ALD, HCHO, NO_x) within a factor 2–3 of their original values. Section 4.3 focuses on model/measurement comparisons for OH and HO₂ using the median campaign measurements and individual days. Finally, section 4.4 provides insights into the radical budget.

4.1 Uncertainties associated with constraining RACM

Several simulations without constraining NO₂, HONO and selected VOCs on individual days and on a median campaign measurements basis were performed in order to determine whether significant errors in the calculated radical concentration could arise from constraining the concentrations of these measured species in the model. There are several reasons for this analysis: (i) HO_x concentrations measured by IU-FAGE depend on local chemistry driven by local concentrations of chemical species. However, several important species used to constrain the model were measured on a larger spatial scale (Table 1) and may not be representative of local concentrations near the IU-FAGE instrument. (ii) Our model assumes unconstrained chemical species to be in photochemical equilibrium (steady-state) to calculate their concentrations. This assumption, which is valid for short-lived species such as RO_x radicals, may not be suitable for unconstrained long-lived species since ambient concentrations of long-lived species are also dependent on physical processes such as deposition, dilution and transport. Miscalculation of the concentration of unmeasured long-lived species that have a direct impact on the radical chemistry may lead to significant errors in calculated radical concentrations. (iii) A shortcoming common to all condensed chemical mechanisms is to constrain the model with a surrogate whose concentration may be underestimated if no measurements are available for the major species.

Several chemical species employed to constrain RACM were measured by LP-DOAS (Table 1) and may not be suitable for local point modeling due to potential concentration inhomogeneities in the probed air mass. Important species are NO₂, HONO, and glyoxal. However, horizontal and vertical gradients were investigated for MCMA-2003 by comparing measurements from two LP-DOAS instruments (Volkamer et al., 2007b). In addition, long path and local point measurements of both O₃ and CO from MCMA-2003 were also compared (Dunlea et al., 2006). These studies led to the conclusion that air masses were well mixed during daytime. This issue was also investigated for this study using the same approach as Volkamer et al. (2007b). HONO concen-

trations measured by two LP-DOAS instruments (DOAS1 and DOAS2) were compared with each other using 30-min median campaign measurements (03/14–03/30). On average, the difference is less than 1.6% from 08:30 a.m. to 06:30 p.m., and this agreement suggests that secondary photochemical species such as HONO are well mixed during the day.

In addition, measured (DOAS2) and RACM-simulated NO₂ concentrations were also compared. Unconstrained simulations of NO₂ resulted in predicted concentrations that were in good agreement with the LP-DOAS measurements between 11:30 a.m. and 05:00 p.m., also consistent with well mixed air masses. However, the model tended to over-predict NO₂ concentrations in the early morning and late afternoon and may suggest inhomogeneous air masses at T0 along the LP-DOAS path. Note that intercomparisons of other species such as O₃ (DOAS2, UV-absorption monitor), SO₂ (DOAS1 and DOAS2) and toluene (DOAS1, PTRMS, Canisters) show good agreement between the different techniques (better than 30% difference for median campaign measurements between 08:30 a.m. and 06:30 p.m.). However, a better agreement is systematically observed during the afternoon, which may suggest the existence of potential inhomogeneities in the concentration of these species during morning hours.

Important unmeasured sources of radicals such as methyl glyoxal (MGLY) and unsaturated dicarbonyls (DCB) exhibit atmospheric lifetimes that are much longer than that for radical species, long enough to invalidate the photochemical equilibrium assumption (Table S5, supplementary material <http://www.atmos-chem-phys.net/9/6655/2009/acp-9-6655-2009-supplement.pdf>). Glyoxal (GLY) was used as a model molecule to investigate a potential miscalculation of other secondary dicarbonyls. Concentrations of glyoxal predicted by unconstrained simulations were compared to that measured by LP-DOAS (DOAS2). Predicted concentrations were higher than that observed by a factor 5–20, suggesting a deviation from the photochemical equilibrium calculated by the model. In addition, Volkamer et al. (2007a) suggested that there may be a missing sink of glyoxal in atmospheric models, likely due to uptake onto aerosols (not described in the chemical mechanism used for this study). These authors used a box model based on the MCM constrained by measured *J*-values and concentrations of VOCs and oxidants (OH, O₃) to predict ambient concentrations of glyoxal during an episode as part of the MCMA-2003 campaign. MCM predicted concentrations of glyoxal were 2–6 times higher than observed, suggesting that there could be missing sinks in the model. These authors suggested that an irreversible uptake onto aerosol surfaces, a reversible partitioning to aerosol liquid water or to oxygenated organic aerosols could account for the missing loss processes. The authors reported that glyoxal uptake onto aerosol surfaces could account for 15% of the SOA formation in MCMA. This missing sink of glyoxal may be linked to an unexpected rapid formation of SOA in MCMA (Volkamer et al., 2006).

In support of the latter statements, a recent study (Volkamer et al., 2009) confirms that glyoxal partitions more efficiently than expected onto the condensed phase. Therefore, it is likely that both a deviation from the photochemical equilibrium and a missing sink of glyoxal contribute to the disagreement observed between measured and predicted glyoxal concentrations in this study. It is important to emphasize that concentrations of other important dicarbonyls likely exhibit a similar behavior. Methyl glyoxal and other α -carbonyl aldehydes (lumped together as MGLY in RACM) and unsaturated dicarbonyls (DCB) were not measured during MCMA-2006 and were calculated by the model. This point is investigated in Sect. 4.2.

Sensitivity tests were also performed to investigate the impact of underestimating the total amount of ketones (KET) and aldehydes (ALD) for this study (Table S6, supplementary material <http://www.atmos-chem-phys.net/9/6655/2009/acp-9-6655-2009-supplement.pdf>). The surrogate KET in RACM lumps acetone and other higher ketones together. For MCMA-2006, only the sum of acetone + propanal was measured by PTRMS. However, measured propanal concentrations are approximately 10 times lower than acetone in the MCMA (Baez et al., 2006), so the sum acetone + propanal was used to constrain KET in our model. Estimations of propanal concentrations for this study using a scaling factor based on measured formaldehyde concentrations (Sheehy et al., 2008) suggest that acetone accounts for more than 90% of the sum at any time of the day. The sensitivity of model-calculated HO_x concentrations to constraining ketones was investigated by increasing [KET] by a factor 2. Predicted HO_x concentrations were less than 1% higher than the base case on an average basis (08:40 a.m.–06:40 p.m.). Because the long lifetime of ketones would lead to a breakdown of the photochemical equilibrium if not constrained (Table S5, supplementary material <http://www.atmos-chem-phys.net/9/6655/2009/acp-9-6655-2009-supplement.pdf>), KET was constrained to acetone measurements for all the simulations presented in this paper. Similarly for the RACM surrogate ALD, which includes higher aldehydes than formaldehyde, Table S6 shows that for an increase of ALD by a factor 3 OH increases by less than 5% while HO₂ increases by 16–21%. These results suggest that errors associated with underestimations of the concentration of these surrogate species would have a minimal impact on calculated HO_x radical concentrations.

4.2 HO_x-sensitivity to model constraints

Simulations performed using the short and large sets of VOCs defined in Sect. 3 led to similar predicted HO_x concentrations and as a result only simulations performed using the large set are presented. Figures 1 and 2 display predicted and measured HO_x concentrations for both the individual days and the median based campaign measurements (14–22 and

27–28 March) respectively. These simulations indicate that both OH and HO₂ are consistently overestimated throughout the day when dicarbonyl species (except glyoxal) are not constrained. OH and HO₂ are overestimated by a factor 2.4 and 1.5 respectively at 01:00 p.m. A close inspection of the radical budget revealed that RO_x radical initiation rates from the photolysis of methylglyoxal (MGLY, unconstrained) and unsaturated dicarbonyls (DCB, unconstrained) are much higher than that derived for glyoxal (GLY, constrained). As mentioned in Sect. 4.1, a shortcoming for these simulations is the severe overprediction of glyoxal when not constrained in the model. It is likely that the same overprediction occurs for other dicarbonyl species such as MGLY and DCB as they exhibit similar sources and sinks. An overestimation of dicarbonyls was observed by Sheehy et al. (2008) and Volkamer et al. (2007b) for 0-D box modeling during MCMA-2003. These authors had to implement additional dilution in their model to avoid an accumulation of oxidized secondary species. This is an important point to address since the reliability of constrained steady-state models relies on measurements of all the long-lived chemical species that influence RO_x concentrations.

Additional modeling was performed for the median campaign measurements and for individual days by assuming that MGLY and DCB undergo similar sinks as glyoxal, although the lifetime of MGLY and DCB are shorter than that for GLY (Table S5, supplementary material <http://www.atmos-chem-phys.net/9/6655/2009/acp-9-6655-2009-supplement.pdf>). The surrogates MGLY and DCB were constrained by scaling predicted concentrations obtained from an unconstrained simulation with the overprediction factor observed for glyoxal. Results for the median campaign measurements are shown in Fig. 2 for both OH and HO₂. When MGLY and DCB are constrained in the model, the agreement between the model and the observations is improved. Around 01:00 p.m., OH is overestimated by less than a factor 1.6 and predicted HO₂ concentrations are generally in good agreement with the measurements. Complementary modeling was also performed by adding an additional first order loss of glyoxal in RACM whose strength was adjusted to bring the predicted glyoxal concentrations into agreement with the measurements. A similar first order loss of MGLY and DCB was also implemented in RACM. On average, when compared to that observed with the scaling procedure, calculated OH and HO₂ concentrations are higher by approximately 9% and 11% respectively on an average basis (08:40 a.m.–06:40 p.m.).

These results highlight the important contribution of secondary oxygenated species to radical initiation in our model and the necessity to correctly characterize the concentration and degradation mechanisms of dicarbonyl species in urban environments. It is likely that the impact of secondary OVOCs on RO_x chemistry is enhanced in urban environments for several reasons: (i) High concentrations of NO_x and primary VOCs lead to a fast cycling of OH, and thus

higher production rates of secondary oxidized species. (ii) HO_x concentrations are much more sensitive to HO_x sources under high NO_x conditions with $[\text{HO}_x] \sim P(\text{HO}_x)^1$ (when HO_x + NO_x reactions dominate radical termination), while under low NO_x conditions $[\text{HO}_x] \sim P(\text{HO}_x)^{1/2}$ (when HO_x self reactions dominate radical termination). As a consequence of the inability of our model to accurately predict dicarbonyl concentrations and the resulting overprediction of HO_x radical concentrations, we chose to use the dicarbonyl-constrained case and the median based campaign measurements in the following discussion unless stated otherwise. Additional sensitivity tests are summarized in Table S6 (supplementary material <http://www.atmos-chem-phys.net/9/6655/2009/acp-9-6655-2009-supplement.pdf>), using the dicarbonyls constrained simulation as the base case.

For MCMA-2003, an intercomparison between measurements of speciated olefins (whole air canister samples and GC/FID) and measurements of total olefins (Fast Olefin Sensor, FOS) showed that 52% of olefins were missing from the canister measurements (Velasco et al., 2007). To investigate the impact of a potential underestimation of olefins on the predicted radical concentrations, modeling was performed by increasing the total concentration of olefins (OLT+OLI) by a factor of 2. These simulations indicated that both OH and HO₂ were higher by 19% and 35% respectively on a daily average (08:40 a.m.–06:40 p.m.). This increase of HO_x in the RACM model is due to two factors: (i) Olefins react with O₃ and lead to the production of RO_x radicals. (ii) In the RACM mechanism, peroxy radicals formed during the OH initiated oxidation of olefins do not form organic nitrates by reaction with NO, which can be a significant sink of radicals. In contrast, peroxy radicals formed during the oxidation of saturated VOCs (HC3, HC5, HC8) can lead to the formation of organic nitrates with a yield of approximately 26% for HC8 in the RACM mechanism. Note that concentrations of HO_x are also more sensitive to olefins than saturated VOCs since the OH-initiated oxidation of one olefin molecule can lead to the production of two molecules of OVOCs such as formaldehyde and higher aldehydes, while only one molecule of OVOCs is formed from the oxidation of saturated VOCs (HC3, HC5, HC8). Secondary OVOCs can photolyze and act as additional sources of radicals.

Simulations performed with the concentration of saturated VOCs (HC3 + HC5 + HC8) increased by a factor 2 resulted with OH decreasing by approximately 11% while HO₂ increased by 15%. In contrast to olefins, HC3-8 does not react with O₃ and does not lead to the production of HO_x radicals. The higher concentrations of saturated VOCs lead to an increase of the OH reactivity, which favor the partitioning of the RO_x radicals into RO₂ and HO₂.

An increase of the constrained CO concentrations by a factor 2 had no impact on the calculated concentrations of OH while RO₂ increased by 4%. The direct cycling of OH through HO₂ via CO does not lead to additional radical losses since HO₂ mainly reacts with NO to reproduce OH. Radical

loss processes involving HO₂ are negligible under the high NO concentrations of MCMA. As for HC3-8, HO₂ increases since an increase of the OH reactivity favors the partitioning of HO_x towards HO₂. An increase of HO_x concentrations observed when increasing HC3-8 and CO is consistent with a VOC sensitive regime.

Formaldehyde can be an important source of radicals in the MCMA (Volkamer et al., 2007b). Sensitivity tests performed by varying the constrained concentrations of HCHO by a factor of 2 resulted in predicted OH and HO₂ concentration changes of –12/+23% and –16/+34% respectively. When HCHO is increased, HO₂ increases faster than OH due to the direct production of HO₂ from HCHO photolysis and an increase of the OH reactivity.

Simulations performed by varying NO_x concentrations by a factor 2 indicated that HO_x concentrations are very sensitive to the concentration of NO_x. Predicted OH and HO₂ concentrations changed in the range +44/–43% and +157/–68% respectively. HO_x concentrations decreased with increasing NO_x, characteristic of a NO_x saturated environment.

Measured $J(\text{HONO})$ values for MCMA-2006 were derived from the recommended absorption cross sections (Sander et al., 2006) and multiplied by 1.43 to be consistent with recent measurements (Volkamer et al., 2007b; Sheehy et al., 2008). In order to assess the impact of this correction, sensitivity tests were performed by dividing constrained $J(\text{HONO})$ values by a factor 1.5. Both OH and HO₂ were lower by 9 and 7% respectively.

Note that in general an increase in the concentration of constraining species leads to an increase of HO_x concentrations except for NO_x. As a result, it is likely that an underestimation of the chemical content of the MCMA atmosphere would lead to an underprediction of the HO_x concentrations.

4.3 Model/measurement comparison of HO_x concentrations

Modeling tests performed in Sect. 4.1 and 4.2 set-up the conditions used to compare predicted and measured HO_x concentrations. The model was constrained with the large set of VOCs, including additional constraints on MGLY and DCB. These simulations are displayed in Figs. 1 and 2 using 10-min time-resolved constraints. Note that simulations performed for the median campaign measurements using 30-min and 60-min time-resolved constraints are similar to that observed for 10-min time-resolved constraints (black line in Fig. 2). In addition, simulations performed using 10-min time-resolved constraints for an average campaign measurements also led to similar results.

4.3.1 HO_x concentrations during morning hours

A close inspection of Fig. 2 indicates that HO₂ is underpredicted during morning hours (08:00 a.m.–11:30 a.m.) for the median campaign measurements, while OH is

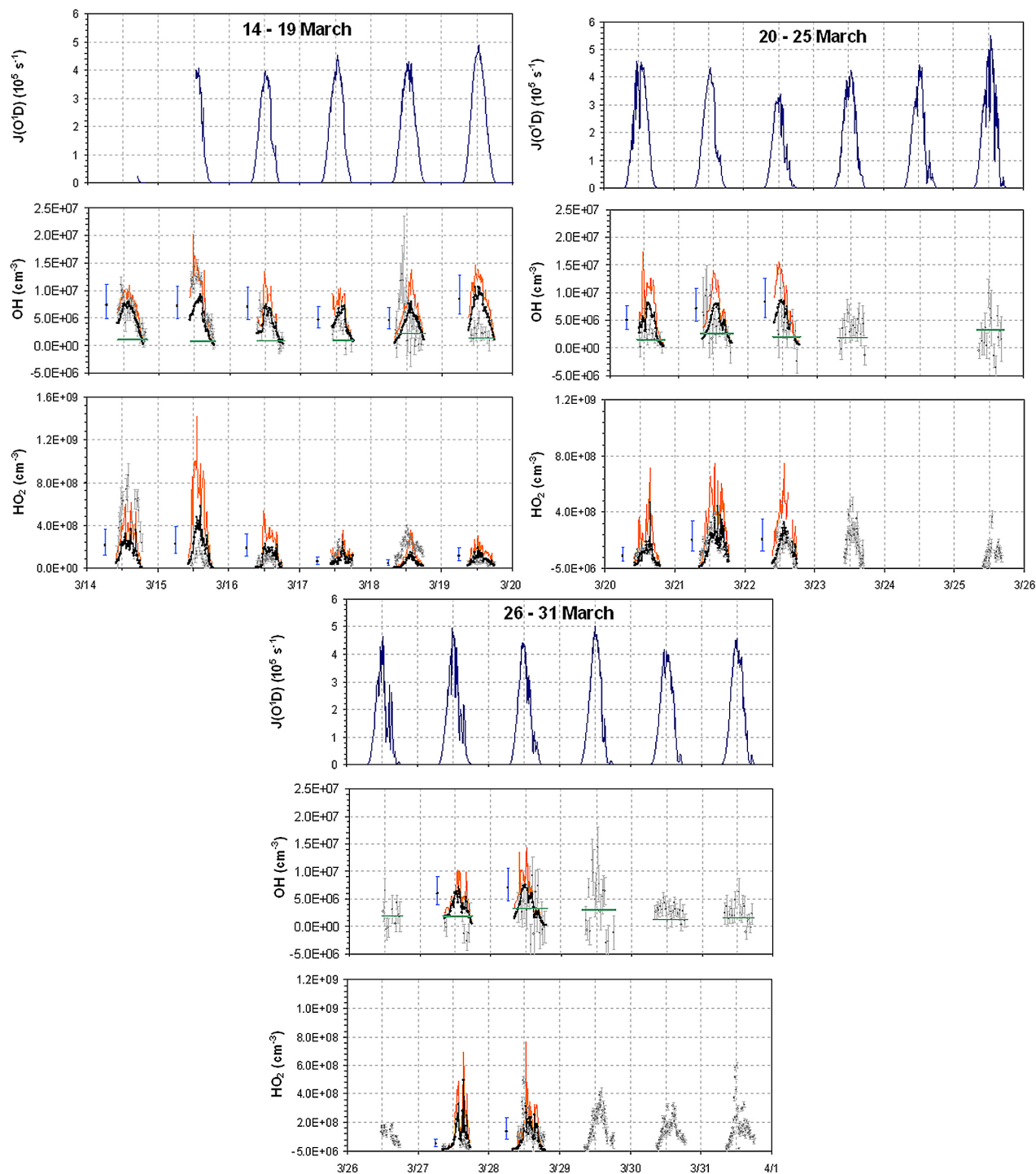


Fig. 1. Measurement/model comparison of HO_x concentrations for individual days. Time is CST. Small grey circles are individual measurements averaged on 7–30 min for OH and 15-s for HO₂. Error bars are the 1σ precision on the measurements. The green line displays the limit of detection ($S/N=1$). 1σ uncertainties on OH and HO₂ calibration factors are $\pm 21\%$ and $\pm 22\%$ respectively. Model-calculated concentrations are displayed for the large set of VOCs as an orange line when MGLY and DCB are not constrained and as a black line when constrained. Blue error bars are model uncertainty for predicted HO_x concentrations at noon (2σ , factors 1.5 and 1.7 for OH and HO₂ respectively) as stated in Sect. 3. Error bars have been shifted to 06:00 a.m. for clarity.

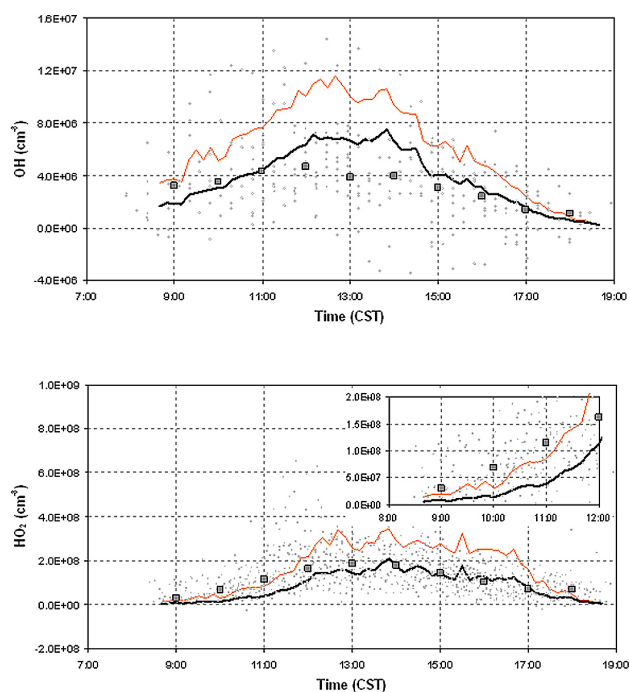


Fig. 2. Measurement/model comparison of HO_x concentrations for the median campaign measurements. Small grey circles are individual measurements from 14 to 31 March (averaged on 30-min for OH and 15-s average for HO₂). Grey squares are median values of these measurements calculated on data binned with a time interval of 1-h. 1σ uncertainties on OH and HO₂ calibration factors are $\pm 21\%$ and $\pm 22\%$ respectively. Orange and black lines are predicted HO_x concentrations (10-min time-resolved constraints, 14–22 and 27–28 March) for unconstrained and constrained dicarbonyls (GLY, MGLY, DCB) simulations respectively.

underpredicted before and overpredicted after 11:00 a.m. The HO₂ underprediction is more severe, and reaches a factor of approximately 5 at 10:00 a.m. Figure 3 shows a direct comparison of the measured and modeled OH and HO₂ concentrations for only the days modeled (14–22 and 27–28 March). While the differences between measured and predicted OH concentrations are not statistically significant (Fig. 3), the disagreement between measured and predicted HO₂ concentrations cannot be explained by model and measurements uncertainties at the 2σ level (Fig. 3). High morning NO concentrations requires elevated production rates of radicals to sustain HO₂ at the observed levels. Several explanations may account for these observations: (i) close emission sources of NO_x and VOCs during traffic hours may lead to inhomogeneous air masses, (ii) an important source of radicals may be missing from the chemical mechanism, (iii) the net HO₂-to-OH propagation rate may be overestimated by RACM due to an unknown chemical process that converts OH into peroxy radicals.

A common assumption of atmospheric models is that the atmosphere is well mixed. However, areas close to emission sources of trace gases are likely inhomogeneous and the

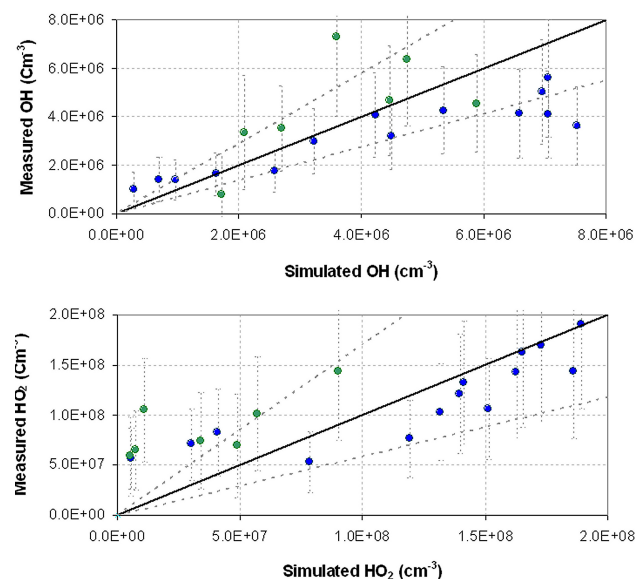


Fig. 3. Measured vs. predicted HO_x concentrations for only the days modeled (14–22 and 27–28 March). Green and blue circles are 30-min median values of OH and HO₂ concentrations characteristic of morning (08:30 a.m.–11:30 a.m.) and afternoon (noon–06:30 p.m.) times respectively. Error bars display the 2σ uncertainty on the measurements by adding precision and calibration uncertainty in quadrature. The black line displays the 1:1 measured-to-modeled ratio while the grey dashed lines display the model 2σ uncertainty on the ratio. Note that the precision of HO₂ measurements (2σ , 3–20%) is better than the calibration uncertainty (2σ , 44%) and thus the error bars for HO₂ reflect a potential systematic error from the calibration rather than random errors on the measurements.

use of kinetic parameters derived from homogeneous measurements may lead to an incorrect description of the kinetic processes occurring in the real atmosphere. Butler et al. (2008) proposed that segregation between OH and isoprene may contribute to the disagreement observed between measured and model-predicted concentrations of OH for the GABRIEL field campaign. Similarly in this study, inhomogeneous air masses are likely present in the morning as discussed in Sect. 4.1. Numerous sources of NO_x and VOCs were present around T0, including vehicular and industrial emissions. Inefficient turbulent mixing and insufficient mixing time during morning hours may also contribute to the formation of inhomogeneous air masses at T0. For this study, it is not trivial to determine to what extent segregation can impact the radical chemistry and how it can affect the partitioning between the different radical species. However, it brings into question the validity of radical modeling in environments close to emission sources. Clearly, further investigations are needed to resolve this issue.

In order to investigate the strength of an additional radical source necessary to explain the high morning HO_x concentrations observed, modeling was performed for 16 March (a day characterized by high morning HO_x concentrations)

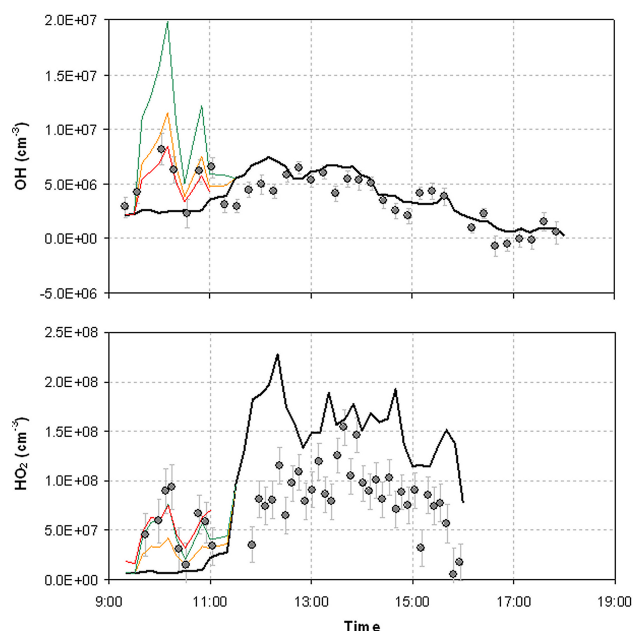


Fig. 4. HO_x concentrations observed on 16 March. Time is CST. Grey circles are individual measurements and error bars are the 1σ precision. Simulations performed using the dataset described in Sect. 3 with additional constraints for MGLY and DCB are displayed by black lines. Orange and green lines represent simulations performed with an additional production of HO₂ in the RACM mechanism for the morning hours (see Sect. 4.3.1). Red lines are simulations performed using an additional production of HO₂ and a reaction rate for HO₂ + NO divided by a factor 2.5 (see Sect. 4.3.1). For 16 March, additional production rates of HO₂ are 1.1×10^8 , 2.2×10^8 and 0.7×10^8 molecule/cm³/s for the orange, green and red lines respectively.

by adding an additional source of HO₂ into the RACM model (Fig. 4). When the strength of this artificial source is adjusted to predict HO₂ concentrations that are in good agreement with the lower limit of that measured (additional HO₂ production of 1.1×10^8 molecule/cm³/s on average), the predicted OH concentrations are in better agreement with observations, suggesting that measured OH and HO₂ concentrations are consistent with each other (orange line in Fig. 4). However, when the strength of this additional source of HO₂ is doubled to match the measurements of HO₂, OH is over-predicted by a factor 1.5–2.5 (green line in Fig. 4). Similar simulations performed for the median campaign measurements were consistent with the conclusions drawn for 16 March. A good agreement between measured and simulated HO₂ concentrations can be obtained for the median campaign measurements by adding an additional production of HO₂ between 08:40 a.m. and 12:00 p.m. (9.4×10^7 molecule/cm³/s on average). This additional production of radicals is equivalent to 1.8 times the initiation rate of RO_x ($\sim 5.2 \times 10^7$ molecule/cm³/s) predicted from the known sources of radicals.

Additional modeling was performed for 16 March as well as the median campaign measurements using an additional production of HO₂ and assuming a slower rate of OH production from the HO₂ + NO reaction. The reason for this approach is to simulate unknown processes that could convert OH into HO₂ under high NO_x conditions, leading to a slower effective rate of HO₂-to-OH conversion. A second reason is the potential segregation between HO₂ and NO discussed above. These simulations are displayed in Fig. 4 for 16 March and show that a very good agreement between measured and simulated OH and HO₂ concentrations can be obtained if the HO₂-to-OH conversion rate is reduced by a factor 2.5 and if an additional production of HO₂ is added in the model (red line in Fig. 4). It is worth mentioning that Shirley et al. (2006) and Sheehy et al. (2008) highlighted a potential imbalance between the OH production and loss rates during morning traffic hours for MCMA-2003 where the OH production rate was higher than the OH loss rate by a factor 2. Note that the rate of HO₂ + NO accounted for more than 80% of the OH production rate for MCMA-2003 (Shirley et al., 2006). Shirley et al. (2006) suggested that some of the products of the reaction between HO₂ and NO are not OH and NO₂, which could either lead to HO_x removal or the regeneration of HO₂ via an additional unknown process. Sheehy et al. (2008) suggested that their model may be missing an HO₂ source that does not form OH. They also mentioned that micro-meteorological phenomena may lead to gas-phase inhomogeneities. In addition, two recent publications also point out a similar imbalance between OH production and loss rates in Santiago, Chile (Elshorbany et al., 2009) and during metropolitan studies performed in US cities (TEXAQS2000, NYC2001, TRAMP2006) (Mao et al., 2009). Note that in the latter studies, this imbalance was derived from measurements of both total OH reactivity and absolute OH concentrations, which allows a direct quantification of the net production and loss of OH in the field.

The T0 site was characterized by elevated concentrations of aromatic species. Toluene and benzene concentrations monitored on the days of elevated morning HO_x observations (16 and 18 March) are amongst the highest recorded during the campaign. During morning traffic hours, benzene and toluene respectively peaked at 8 and 70 ppb on 16 March and at 18 and 24 ppb on 18 March, while benzene and toluene median mixing ratios observed from 14 to 31 March were 5 and 24 ppb respectively.

The chemical mechanism of aromatic oxidation in the atmosphere is poorly understood (Bloss et al., 2005b) and chamber experiments performed during the EXACT project in the EUPHORE atmospheric chamber showed that HO_x radical concentrations were severely underpredicted by a model based on the Master Chemical Mechanism (MCM v3.1). Experiments performed on the photo-oxidation of toluene under similar NO_x conditions as that observed during morning rush hours during MCMA-2006 but with higher concentrations of toluene (approximately 500 ppb) showed

that an additional source of radicals was required to explain the oxidative capacity of this aromatic system. The strength of the additional source (4×10^8 molecule/cm³/s) was similar to that necessary to explain the MCMA-2006 field observations of HO₂ described above. It is possible that the inability of atmospheric models to reproduce the oxidative capacity of aromatics may be responsible for some of the morning underestimation of HO_x concentrations during the MCMA-2006 field campaign.

The higher-than-expected HO₂ measured under high NO_x conditions has also been observed previously in the MCMA. Sheehy et al. (2008) performed a detailed modeling study to characterize the RO_x radical chemistry during MCMA-2003. Results from a highly constrained model based on the Master Chemical Mechanism showed that measured morning OH and HO₂ concentrations (until 10:00 a.m.) were underestimated by a factor 2 and 5–10 respectively. Similar model/measurement discrepancies have also been reported in the literature from other urban field campaigns. Martinez et al. (2003) indicated that the HO₂-NO dependence observed from measurements performed during the SOS campaign in Nashville (summer 1999) was not reproduced by their model based on a lumped chemical mechanism. The model predicted a faster decrease of HO₂ with increasing NO. Ren et al. (2003) showed that in New York City (summer 2001), HO₂ predictions from a model based on RACM were in good agreement with measurements for NO < 5 ppb. However, measured HO₂ concentrations were underestimated by a factor 2–20 for NO mixing ratios higher than 20 ppb. Kanaya et al. (2007) also observed higher HO₂ concentrations than predicted by their RACM model under high NO_x conditions during a field campaign performed in Tokyo. An additional source of radicals (1×10^7 molecule/cm³/s at 20 ppb NO for the winter campaign) was necessary to resolve the disagreement between measured and predicted HO₂ concentrations. The results presented here from the MCMA-2006 field campaign are consistent with these previous urban measurements and suggest that an unknown source of radicals, whose strength may be scalable to NO_x (Kanaya et al., 2007), may be missing from current atmospheric chemistry models.

4.3.2 HO_x concentrations during afternoon hours

On a median basis, measured HO_x concentrations are reasonably well reproduced by the model after 11:30 a.m. OH concentrations are over-predicted by roughly a factor 1.7 from 11:30 a.m. to 02:30 p.m. and are in good agreement with observations after 02:30 p.m. While these discrepancies are within measurement-model uncertainties, this overestimation of OH around solar noon has also been observed during other urban field campaigns (George et al., 1999; Platt et al., 2002; Emmerson et al., 2007; Volkamer et al., 2007b; Sheehy et al., 2008), using models based on either a condensed or an explicit chemical mechanism. Note that HO₂ was also over-predicted for three of the studies mentioned

above (George et al., 1999; Platt et al., 2002; Emmerson et al., 2007) while HO₂ is well reproduced by our model from 11:30 a.m. to 05:00 p.m. In contrast, a few studies (Martinez et al., 2003; Ren et al., 2003; Emmerson et al., 2005a) exhibit an underprediction of both OH and HO₂ using either MCM or a lumped mechanism.

Missing OH reactivity from saturated chemical species cannot account for a large overestimation of OH around noon due to a rapid recycling of OH from RO₂+NO and HO₂+NO (see Fig. 8). An increase of the constrained concentrations for HC3+HC5+HC8 by a factor two only leads to 8–13% decrease of OH (see Table S6, supplementary material <http://www.atmos-chem-phys.net/9/6655/2009/acp-9-6655-2009-supplement.pdf>), while the measured concentrations are a factor 1.7 lower than predicted. In addition, missing reactivity from unsaturated species would lead to a larger disagreement between measured and predicted OH concentrations around noon as shown by a simulation performed with a 2-fold increase of OLT and OLI in the model (see Table S6, supplementary material <http://www.atmos-chem-phys.net/9/6655/2009/acp-9-6655-2009-supplement.pdf>). OH increases by 11–23% in the latter simulation.

Photo-oxidation experiments of unsaturated dicarbonyl species (DCB) showed that MCM v3.1 underestimates HO₂ concentrations by an order of magnitude under high NO_x conditions, while DCB photolytic experiments indicated that MCM overestimates HO₂ by an order of magnitude under NO_x free conditions (Bloss et al., 2005b). Interestingly, glyoxal is over-predicted by a factor 3–4 in both cases. These experimental results highlight a poor characterization of the dicarbonyl chemistry in actual atmospheric models, and may explain the measurement/model discrepancies near local noon.

A recent update of the MCM mechanism (Bloss et al., 2005a) emphasize several shortcomings regarding the photochemistry of unsaturated dicarbonyl species (DCB). For the present study, the DCB chemistry included in the model was that proposed by Stockwell et al. (1997). However, there are several differences between the RACM model and MCM v3.1. Based on recent findings, Bloss et al. (2005b) updated the MCM v3.1 with a higher photolysis rates for DCB species containing an aldehyde group ($J(\text{DCB}) = 0.2 \times J(\text{NO}_2)$). Note that the J -value parameterization used in MCM v3.1 leads to values that are three times higher than that used in the RACM model from this study. In addition, RACM only considers one product channel for the photolysis of DCB species, leading to the formation of unsaturated acylperoxy radicals (TCO₃) and HO₂ (R1a), while MCM incorporates a second channel for the production of furanone type species (R1b), with a branching ratio $k_{1a}/(k_{1a} + k_{1b}) = 0.6$:



Additional simulations were performed for the median campaign measurements using an updated chemical mechanism including the above mentioned recommendations. The subsequent chemistry (R2–R6) was also added to RACM to describe the fate of the furanone type species produced in R1b. The rate constants, branching ratios and *J*-values were set as defined in MCM v3.1.



These modified simulations led to similar predicted HO_x concentrations, with calculated OH and HO₂ concentrations different by less than 3% than that predicted by the non-updated model. In terms of radical production strength, the lower *J*(DCB) values used in the RACM model are compensated by the missing channel that leads to the production of non-radical species. However, due to a shorter calculated lifetime of DCB species with respect to photolysis, the predicted DCB concentrations decrease by approximately a factor 2–2.5 for the simulations performed with the updated mechanism. Although this additional chemistry may not explain the model/measurement disagreement near local noon, it may explain some of the overprediction of DCB species in the model. Clearly additional studies of the photochemistry of unsaturated dicarbonyl species are still needed to help resolve some of these discrepancies.

A close inspection of Fig. 3 suggests that HO₂ concentrations measured from 05:30 to 06:40 p.m. (blue circles for HO₂ concentrations lower than $5 \times 10^7 \text{ cm}^{-3}$) are underestimated by RACM. An underprediction of HO₂ during the late afternoon may be due to an unaccounted source of radicals. However, note that only one HO₂ measurement is significantly different from the simulated concentrations and unfortunately no HO₂ measurements were performed after 07:00 p.m. Further discussion on a potential underestimation of HO₂ in the late afternoon would be only speculative.

Simulations performed using median campaign concentrations do not provide information about the ability of the model to reproduce the day-to-day variations of HO_x concentrations. Figure 1 illustrates this behavior for daily modeling and shows that the level of agreement is worse for both OH and HO₂ than that observed for the median campaign measurements. Good agreement for OH is observed on 14

and 16 March (afternoon), while the measured OH concentrations are underpredicted on March 15 and the mornings of 16, 18 and 21 March, and over-predicted the rest of the campaign. Good agreement for HO₂ is observed on 20–22 and 28 March while the measured concentrations are underpredicted on 14, 16 (morning), 17–18 March and overpredicted on 15, 16 (afternoon) and 19 March. In addition, characteristics such as the decrease of HO₂ from 14 to 15 March, the increase of HO₂ from 17 to 18 March and the shape of the diurnal profile are not well reproduced by the model. However, measurements and model prediction agree within 2σ uncertainties for most of the days, except for 14 (HO₂), 15 (HO₂, OH), 16 (HO₂), 18 (HO₂) and 19 March (OH). The better agreement observed using median concentration profiles is likely the result of error cancellation for both measured and predicted HO_x concentrations. Using measured median profiles of HO_x concentrations improves the precision of the measurements, while for predicted HO_x concentrations the model overprediction observed on some days is cancelled by the underprediction observed on other days.

The overall agreement observed for the median campaign measurements is consistent with that observed during MCMA-2003 (Shirley et al., 2006; Sheehy et al., 2008). However, it should be noted that the reported concentrations for MCMA-2003 have recently been revised and the new concentration profiles are approximately 1.6 times greater than previously reported (Mao et al., 2009). As a result, modeling studies performed for MCMA-2003 (Shirley et al., 2006; Volkamer et al., 2007b; Sheehy et al., 2008) underpredict the revised concentrations of both OH and HO₂.

4.3.3 HO₂/OH ratios

Urban environments are characterized by a fast radical cycling due to high NO concentrations, and the radical partitioning between OH, HO₂ and RO₂ occurs rapidly relative to variations in the RO_x initiation and termination rates. As a consequence, the HO₂/OH ratio does not depend on the strength of the RO_x sources and sinks and is a good indicator of our understanding of the reactions involved in the propagation of radicals. Simulations performed by either constraining only glyoxal or all the dicarbonyl species lead to similar HO₂/OH ratios and are consistent with this ratio reflecting radical propagation in the model.

Measured and predicted HO₂/OH ratios are displayed in Fig. 5 as a function of NO. On average, the agreement is good during the afternoon when NO ranges from 1 to 5 ppb. On the other hand, the model underestimates the measured ratios by approximately a factor 2 around 10 ppb of NO typically observed in the late morning. This disagreement increases with increasing NO, and predicted ratios are lower than observations by roughly a factor 5–6 at NO levels of 100 ppb often observed in the early morning. This behavior is consistent with that observed for MCMA-2003. For 100 ppb of NO, Shirley et al. (2006) and Sheehy et al. (2008)

report a modeled HO₂/OH ratio that is lower than the measurements by a factor 2 and 4 respectively. In addition, the MCMA-2003 HO₂/OH vs. NO relationship exhibits a power dependence of 0.64 and 0.36 for the model-calculated and measured ratios respectively (Sheehy et al., 2008), similar to the MCMA-2006 power dependence for both RACM (0.78) and the measurements (0.28) reported here. Note that for MCMA-2003, the revision of the HO_x concentrations mentioned above does not affect the HO₂/OH ratio significantly as similar correction factors are applied for both OH and HO₂.

The tendency of models to underestimate HO₂/OH at high NO has also been observed during other urban field campaigns (Ren et al., 2003; Emmerson et al., 2005a). Additional simulations were performed by increasing the concentrations of HC3, HC5, HC8, OLT and OLI by a factor 2 to investigate if some missing OH reactivity could explain the disagreement between measured and simulated HO₂/OH ratios. The simulated ratios are displayed by the green line in Fig. 5. It is clear that a 2-fold increase of the concentration of these surrogates cannot explain the HO₂/OH ratios observed under high NO conditions. The NO dependence remains unchanged and the agreement between measured and simulated ratios under low NO mixing ratios (1–3 ppb) is worse.

As mentioned in Sect. 4.3.1, simulations performed with a lower production of OH from the HO₂ + NO reaction are in better agreement with observations. HO₂/OH ratios from these simulations (not shown) are in better agreement with observations for NO > 20 ppb and support the hypothesis that the effective HO₂-to-OH propagation rate may be overestimated by the model. A process converting OH into peroxy radicals may be missing from the chemical mechanism and/or incomplete mixing of the air mass may lead to segregation between HO₂ and NO.

4.4 Radical budget analysis

A rate of production analysis (Emmerson et al., 2005b) was carried out for the morning (08:40 a.m.–11:50 a.m.), early afternoon (12:00 p.m.–15:50 p.m.), late afternoon (16:00 p.m.–18:40 p.m.) and on a daily average (08:40 a.m.–18:40 p.m.). This analysis consists of investigating the key processes driving RO_x initiation, termination and cycling. The results discussed below and displayed in Figs. 6–8 and Tables S3–S4 (supplementary material <http://www.atmos-chem-phys.net/9/6655/2009/acp-9-6655-2009-supplement.pdf>), are from simulations performed with the median campaign measurement dataset and the dicarbonyl species (GLY, MGLY, DCB) constrained. In the following discussion, radical “initiation” refers to the production rate of a specific radical from closed shell molecules due to photolytic processes or chemical reactions. Radical “production” refers to the production rate of a specific radical, from initiation and propagation rates of other radical species. Note that the calculations presented

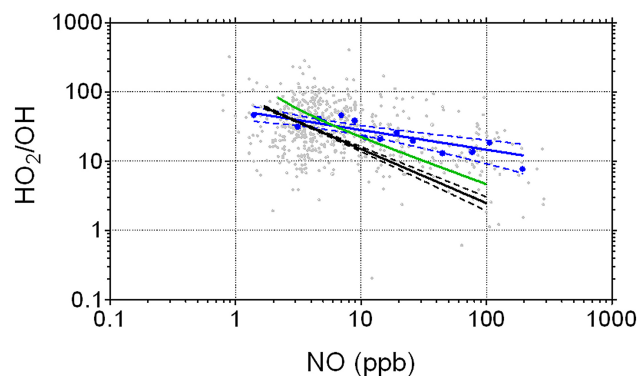


Fig. 5. Correlation plot for HO₂/OH vs. NO. Small grey circles are individual measurements recorded for the whole campaign. Large blue circles are median values calculated on binned NO data and the blue line is a fit to the median measurements. Model-calculated ratios are displayed by a black line for the median campaign measurements. Dashed lines are the 95% confidence interval from the non-linear power regressions. The green line represents the model-calculated ratios from a simulation performed with a two-fold increase of the concentrations of the surrogates HC3, HC5, HC8, OLT and OLI.

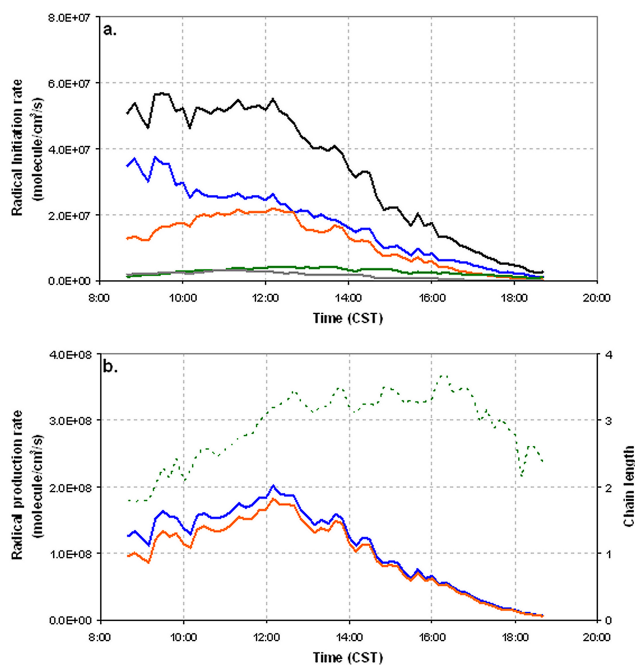


Fig. 6. Model-calculated rates of radical initiation, production and chain length for the median campaign measurements. (a) The blue, orange, green and grey lines display the initiation rates of OH, HO₂, RO₂ and RCO₃ respectively. The black line represents the total initiation rate of RO_x (OH + HO₂ + RO₂ + RCO₃). (b) The blue and orange lines display the production rates of OH and HO₂ respectively. These production rates account for both initiation and propagation of the radicals. The calculated chain length is displayed as a dotted green line.

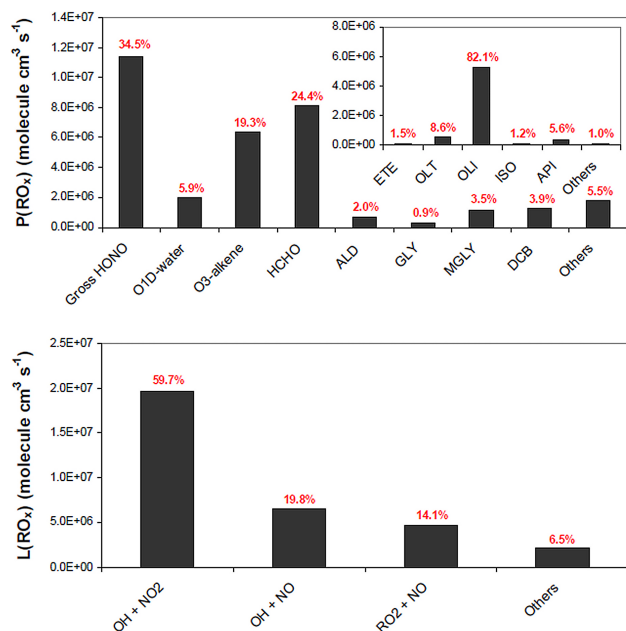


Fig. 7. Model-calculated rates of RO_x initiation and termination averaged between 08:40 a.m. and 06:40 p.m. The insert in the top panel displays a breakdown of the O₃-alkene contribution. Note that these calculations are based on a gross initiation rate of OH from HONO photolysis. The contribution of HONO photolysis to the total rate of RO_x initiation would be smaller on a net basis.

below and in Tables S3 and S4 are based on the gross OH initiation rate from HONO, calculated as $J_{\text{HONO}} \times [\text{HONO}]$.

For the MCMA-2003 field campaign, Volkamer et al. (2007b) pointed out that the peak of radical initiation does not necessarily track the available light as might be expected if photolytic processes are the main drivers of radical initiation. This is a consequence of high morning concentrations of secondary oxygenated species such as HONO, HCHO and dicarbonyl species, which tend to amplify the radical production in the morning. Figure 6a displays the radical initiation rates of RO_x radicals during MCMA-2006 for the median campaign measurements. These rates exhibit a broad peak at approximately 5.2×10^7 molecule/cm³/s between 08:40 a.m. and noon. Initiation rates of OH and HO₂ show similar contributions after 11:00 a.m. while initiation of OH is approximately twice higher than HO₂ on average before 11:00 a.m. The initiation rate of peroxy radicals (RO₂ + RCO₃) accounts for 1/7th of the total RO_x initiation rate. These results are consistent with the radical budget analysis performed for MCMA-2003 (Volkamer et al., 2007b) using a model based on a more comprehensive mechanism (MCM v3.1). MCM predicted a peak of radical initiation of approximately 6.2×10^7 molecule/cm³/s around 10:00 a.m. with similar contributions from the initiation of OH and HO₂, and a lower contribution of RO₂ + RCO₃.

Figure 6b displays production rates of OH (P(OH)) and HO₂ (P(HO₂)) and the chain length (CL) for OH. The chain

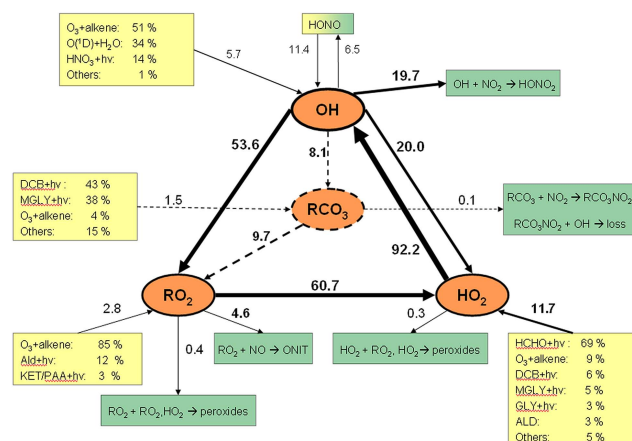


Fig. 8. Rate of production analysis performed for the median campaign measurements from 08:40 a.m. to 06:40 p.m. These calculations are based on measured concentrations of VOCs, NO_x and inorganic species and model-predicted concentrations of radicals. Initiation, termination and propagation rates are in 10⁶ molecule/cm³/s. The percentage values represent the contribution of each process to the rate.

length was calculated as the ratio of the HO₂-to-OH propagation rate over the total RO_x termination rate. P(OH) and P(HO₂) peak around 12:30 p.m. at approximately 1.8×10^8 molecule/cm³/s while a maximum CL of 3.0–3.5 is observed between 12:30 and 05:00 p.m. With propagation rates higher than initiation rates during the day, it is clear that radical propagation controls the radical concentrations in MCMA. The chain lengths derived from these simulations are consistent with those observed for MCMA-2003 (Sheehy et al., 2008). Using MCM v3.1, Sheehy et al. calculated chain lengths in the range 2.5–4.0, taking into account the propagation efficiency of OH through the RO₂ and HO₂ compartments. Since the production rate of OH is dominated by the rate of HO₂ + NO (86% on a daily average), the chain length almost reaches its maximum when P(OH) is the highest, which corresponds to the maximum propagation rate from HO₂ + NO at 12:30 p.m. However, similar relative decreases of both the OH-propagation rate from HO₂ + NO and the total RO_x termination rate sustain the chain length from approximately 12:30 p.m. to 05:00 p.m.

On a daily basis (08:40 a.m.–06:40 p.m.), the RO_x initiation is dominated by the formation of OH (52%), HO₂ (35%), RO₂ (8%) and RCO₃ (5%). In the late afternoon, the RO₂ contribution increases to 21% with OH, HO₂ and RCO₃ contributing to 50%, 26% and 3% respectively. Individual processes leading to the RO_x initiation in MCMA are displayed in Table S3 (supplementary material <http://www.atmos-chem-phys.net/9/6655/2009/acp-9-6655-2009-supplement.pdf>). The main initiation processes for OH are HONO photolysis (67%), O₃-alkene reactions (17%) and O₃ photolysis (11%). Note that HNO₃ photolysis contributes to 5% of the OH initiation rate.

HNO₃ was not constrained for this study and no corrections were applied for a potential breakdown of the photochemical equilibrium due to transport and partitioning onto aerosols (Zheng et al., 2008). Gas-phase concentrations of HNO₃ predicted by our model are likely overestimated. However, the low contribution of HNO₃ to the total initiation rate of RO_x radical does not alter the conclusions of this study. Other intermediate species that are not constrained (H₂O₂, OP1, OP2, PAA, ORA1, ORA2, CSL, MACR, UDD, HKET) have a negligible impact on the production and loss rates of RO_x.

HO₂ is initiated by HCHO photolysis (69%), O₃-alkene reactions (9%) and photolysis of dicarbonyl species (14%). Initiation of RO₂ occurs from O₃-alkene reactions (85%) and photolysis of aldehydes higher than HCHO (12%). For RCO₃, photolysis of dicarbonyl species accounts for 81% of the initiation rate.

On a daily basis (08:40 a.m.–06:40 p.m.), the main sources of RO_x radicals (Fig. 7) are photolysis of HONO (35%), photolysis of HCHO (24%), O₃-alkene reactions (19%) and photolysis of dicarbonyl species (8%). Note that the production of OH from O(¹D)+H₂O only contributes to 6% of the total RO_x initiation rate. In the late afternoon (04:00 p.m.–06:40 p.m.), O₃-alkene reactions contribute to more than 56% of the RO_x initiation rate, due to the decreasing rates of the photolytic processes with decreasing solar light intensity.

These results highlight the important contribution of HONO photolysis and O₃-alkene reactions to radical initiation during MCMA-2006, and are different from a source apportionment performed for MCMA-2003 (Volkamer et al., 2007b). On a daily average basis (06:00 a.m.–06:00 p.m.), Volkamer et al. (2007) predicted contributions of HONO photolysis, O₃ photolysis, HCHO photolysis and O₃-alkene reactions to the total RO_x initiation rate of 13, 21, 21, and 14%, respectively, with the contribution due to HONO photolysis approximately 2–3 times smaller than predicted in this study. Their model also predicted a contribution of approximately 25% for the photolysis of secondary OVOCs (dicarbonyls, aldehydes higher than HCHO, ketones), which is approximately twice larger than that predicted in this study. Interestingly, absolute production rates of OH, HO₂ and (RO₂ + RCO₃) derived for MCMA-2003 and 2006 are similar regardless of the specific sources.

Different sampling locations are likely the reason for the differences observed in the radical budget. For instance, O₃ photolysis is of minor importance during MCMA-2006 while it contributes to 21% of the total RO_x initiation rate in 2003. This is mainly due to high NO_x concentrations observed at T0 (median morning peak of 250 ppb) compared to CENICA (86 ppb). During the morning and early afternoon, O₃ is efficiently titrated by NO at T0 and peaks around 02:00–02:30 p.m. (Dusanter et al., 2008) while *J*(O¹D) peaks sooner around 12:30 p.m. (CST). Note that at 02:30 p.m. *J*(O¹D) is half its peak value and the production of OH from O₃ photolysis is already declining. In 2003, the sim-

ilar timing between *J*(O¹D) and O₃ (12:00–12:30 p.m.) led to higher production rates of OH from O₃ photolysis.

The higher contribution of HONO observed for MCMA-2006 is a result of high ambient concentrations of HONO measured at T0. Note that the photolytic loss of HONO calculated from the measured HONO concentrations and *J*(HONO) is systematically higher than the HONO production rate from OH+NO throughout the day. On a daily basis (08:40 a.m.–06:40 p.m.), the loss rate of HONO from photolysis is 11.4×10⁶ molecule/cm³/s while the production rate from OH+NO is 6.5×10⁶ molecule/cm³/s. This imbalance between loss and production rates suggests that there may be an additional source of HONO whose strength is similar to that observed for the homogeneous gas-phase production from OH+NO. The higher NO_x concentrations observed at the T0 site may also be responsible for this missing source of HONO. A body of growing evidences suggests that an unknown source of HONO is occurring in the troposphere, likely due to light-enhanced heterogeneous reactions of NO₂ on surfaces (Kleffmann, 2007). This issue will be further investigated for MCMA-2006. The important contribution of HONO photolysis to the radical initiation was also observed for New York City (Ren et al., 2003) and Santiago (Chile) (Elshorbany et al., 2009). On average, HONO photolysis accounted for 56% of the HO_x initiation during daytime in New York City and 55% of the total OH initiation rate in Santiago.

A recent study from Li et al. (2008) suggested that the reaction of excited NO₂ molecules with water-vapor could be an important source of OH that is missing from current models of atmospheric chemistry. These authors suggested that the OH initiation rate from this source may be as high as 50% of the OH initiation rate from O₃ photolysis at high solar zenith angles. For a clean environment (NO₂~400–1000 ppt), the OH initiation rate from NO₂*+H₂O was estimated to be in the range 5×10³ to 4×10⁴ molecule/cm³/s. In addition, Wennberg and Dabdub (Wennberg and Dabdub, 2008) showed that the inclusion of this OH production channel in air quality models of the Los Angeles basin was responsible for an increase of up to 30–40% of the calculated O₃ concentrations throughout the city.

This additional source of OH is expected to have a strong impact on environments characterized by high concentrations of NO₂, such as the MCMA. Additional modeling was performed for March 14 including the following chemistry in the RACM model:



The rate constants used were $k_8 = 3.3 \times 10^{-11}$, $k_9 = 2.7 \times 10^{-11}$, $k_{10a} = 1.7 \times 10^{-10}$, $k_{10b} = 1.7 \times 10^{-13}$ cm³ molecule⁻¹ s⁻¹. Time-resolved photolysis frequencies for R7 were calculated using NO₂ absorption cross sections, quantum yields for the production of excited molecules of NO₂ and values of the actinic flux (320–645 nm). Absorption cross sections and quantum yields were taken from the Tropospheric Ultraviolet-Visible (TUV 4.4) model (Madronich, 1989; Madronich and Weller, 1990). Quantum yields for the production of excited molecules of NO₂ were assumed to be $1 - \Phi$ where Φ is the quantum yield for the photodissociation of NO₂. The actinic flux was calculated by TUV 4.4 for 14 March at the coordinates of T0.

Using the modified RACM model, predicted OH and HO₂ concentrations are higher by less than 1% than that predicted without excited NO₂ chemistry. A rate of production analysis indicated that the OH initiation rate from NO₂* + H₂O is equivalent to 18% of the OH initiation rate from O₃ photolysis between 9:50 a.m. and 10:50 a.m. On average, O₃ photolysis and NO₂* + H₂O lead to initiation rates of 2.0×10^6 and 3.5×10^5 molecule/cm³/s respectively. On a daily basis (09:50 a.m.–06:30 p.m.), the OH initiation rate from NO₂* + H₂O is equivalent to 6% of the OH initiation rate from O₃ photolysis. However, O₃ photolysis is not the main source of radicals during MCMA-2006 and its contribution to the initiation rate of RO_x radicals is small. As a consequence, the relative importance of the NO₂* + H₂O channel to the RO_x initiation rate is negligible for MCMA-2006 where other radical sources dominate.

It is worth noting that this new source of OH is still questionable. A previous study using a pulsed-laser-excitation/resonance fluorescence technique reported that the reactive quenching of NO₂* by water was negligible under tropospheric conditions and that OH was produced by a 2-photon absorption sequence leading to the production of excited oxygen atoms (O¹D) that then react with water to produce OH (Crowley and Carl, 1997). These authors derived a rate constant for Reaction (10b) of approximately 1.2×10^{-14} cm³/molecule/s, 14 times slower than that derived in the study of Li et al. (2008). In addition, a recent study (Carr, 2009) using a laser-induced fluorescence technique to detect OH also report an OH yield for Reaction (10b) that is 17 times lower than that observed by Li et al. (2008). In this paper, we demonstrate that if this new source of OH radicals occurs in the troposphere, its contribution to the total rate of OH initiation is negligible in the MCMA.

The RO_x termination is dominated by OH + NO_x reactions and to a smaller extent by RO₂ + NO (Fig. 7). These reactions lead to the production of nitric acid (HNO₃), nitrous acid (HONO) and organic nitrates. Table S4 (supplementary material <http://www.atmos-chem-phys.net/9/6655/2009/acp-9-6655-2009-supplement.pdf>) displays the contribution of the main sinks throughout the day. On a daily average (08:40 a.m.–06:40 p.m.), OH + NO₂, OH + NO, and

RO₂ + NO account for approximately 60%, 20% and 14% of the total RO_x termination respectively. Note that additional sinks are grouped together under the label “Others” in Fig. 7. Both radical-radical reactions and HNO₃ + OH account for approximately 50% of this additional sink. As mentioned earlier, concentrations of HNO₃ are likely overestimated since no corrections were applied for a potential breakdown of the photochemical equilibrium. However, the small overestimation of both the initiation and termination rates of OH from the overprediction of HNO₃ likely compensate each other and do not alter the conclusions of this study. For instance, the total initiation and termination rates of OH from HNO₃ for the median campaign measurements (08:40 a.m.–06:40 p.m.) are 8.0×10^5 and 1.1×10^6 molecule/cm³/s respectively. A net total loss of OH of 3.0×10^5 molecule/cm³/s is derived for the median campaign measurements. This flux of OH is negligible compared to the radical fluxes displayed in Fig. 8.

Radical losses through the RCO₃ compartment depend on the formation of peroxy acetyl nitrate (PAN) species and subsequent reactions with OH. The loss of radicals calculated by the model depends on the competition between the thermal decomposition of PANs and their reaction with OH. During MCMA-2006, this sink was negligible on a daily basis (0.1×10^6 molecule cm⁻³ s⁻¹) compared to the propagation toward RO₂ (9.7×10^6 molecule cm⁻³ s⁻¹). However, note that lower ambient temperatures would lead to a decrease of the thermal decomposition rate and an increasing contribution of the latter sink to the total RO_x termination rate.

Daily averages (08:40 a.m.–06:40 p.m.) of initiation, termination and propagation rates of RO_x radicals are shown in Fig. 8. Initiation and termination rates are roughly in balance at 3.3×10^7 molecule cm⁻³ s⁻¹, consistent with the MCMA-2003 radical budget (Volkamer et al., 2007b). As pointed out for MCMA-2003 (Volkamer et al., 2007b), the RO_x termination rates observed during MCMA-2006 are approximately one order of magnitude higher than the rates observed in other urban environments (Emmerson et al., 2005b, 2007). However, elevated RO_x termination rates are compensated by higher production rates of radicals due to the photolysis of secondary oxygenated species such as HONO, HCHO, OVOCs and O₃-alkene reactions. This compensation sustains an efficient photochemistry in the MCMA.

5 Conclusions

A zero-dimensional box model, based on the Regional Atmospheric Chemical Mechanism (RACM), was constrained by 10-min average of 24 *J*-values and the concentrations of 97 chemical species. This model was used to predict the concentration of RO_x radicals (=OH + HO₂ + RO₂) and their rates of initiation, propagation and termination. This study highlights the challenge of using photochemical 0-D box models to investigate the radical chemistry in highly polluted environments. These models are required to be constrained by a

suite of measurements including all the long-lived chemical species influencing the radical chemistry. In addition, inhomogeneities in the concentration of gas-phase species may complicate the zero dimensional approach used for free radical modeling in urban environments with numerous sources of emissions. The MCMA-2006 campaign was a unique opportunity to test the ability of current atmospheric chemistry models to reproduce the observed radical concentrations given the comprehensive measurement suite obtained during the campaign.

In general, the base RACM model consistently overestimated the concentrations of both OH and HO₂ throughout the day when dicarbonyls species are not constrained. For MCMA-2006, only glyoxal was measured by LP-DOAS and glyoxal-unconstrained simulations indicated that the model overestimates its concentration. The reason is likely a breakdown of the photochemical equilibrium assumption due to the absence of transport in the zero dimensional approach and a missing sink of glyoxal in atmospheric models as suggested in previous studies. In order to prevent a miscalculation of the radical concentrations, the model was constrained by the observed concentrations of glyoxal, with additional constraints on the estimated concentrations of methylglyoxal and unsaturated dicarbonyl species which can also act as radical sources. The agreement between measured and modeled HO_x concentrations is improved with these constraints, and as a result future field campaigns would benefit from accurate measurements of these compounds.

Based on the dicarbonyls-constrained simulations, HO₂ was underpredicted during morning hours (08:40–11:30), consistent with previous urban field campaigns. This study adds support to an increasing body of evidence suggesting that a significant source of radicals is missing from current atmospheric models of polluted environments. Because elevated morning concentrations of HO_x were observed on days when the measured concentrations of toluene and benzene were higher than that observed on other days, it is postulated that this missing source may be linked to the poorly characterized oxidative capacity of aromatics under high NO_x conditions, consistent with previous atmospheric chamber measurements of toluene oxidation. Additional studies of the atmospheric oxidation of aromatics and secondary oxygenated species are still needed to improve our understanding of the oxidative capacity of polluted environments.

In contrast to the morning observations, HO₂ is well reproduced by the model in the afternoon while OH is overestimated by roughly a factor of 1.7 around noon but is in good agreement with the observations after 02:30 p.m. However, predicted HO₂/OH ratios are underestimated for NO mixing ratios higher than 5 ppb, also consistent with previous urban field campaigns. The latter point suggest that the net HO₂-to-OH propagation rate may be overestimated by the model and a process converting OH into peroxy radicals, likely linked to NO_x chemistry, may be missing from the chemical mechanism.

An investigation of the radical budget indicates that radical initiation in the MCMA is the result of several photolytic and non-photolytic processes. On a daily basis (08:40 a.m.–06:40 p.m.), the model predicts that photolysis of HONO (35%), photolysis of HCHO (24%), O₃-alkene reactions (19%) and photolysis of dicarbonyls (8%) are the main sources of radicals. O₃-alkene reactions are predicted to be even more important in the late afternoon (04:00–06:40 p.m.), contributing to more than 56% of the total RO_x initiation rate. Production of OH from O(¹D) + H₂O was found to be marginal for MCMA-2006 and accounted for only 6% of the RO_x initiation rate. In addition, OH initiation from excited NO₂ chemistry was found to be negligible. Predicted radical propagation rates are an order-of-magnitude greater than the calculated radical initiation rates throughout the day, and control the oxidative capacity of the atmosphere in the MCMA.

Overall, despite differences in model implementation and constraints for this study and the studies performed for MCMA-2003, the degree of agreement is good. Consistent with previously published urban field campaigns, the morning model-underestimation of HO_x concentrations and HO₂/OH ratios suggests that our understanding of the fast HO_x photochemistry under high NO_x conditions is still incomplete. Additional measurements of HO_x radicals are still needed to improve our understanding of the oxidative capacity of polluted urban environments.

Acknowledgements. The authors are grateful to Xinrong Ren and Philip Sheehy for helpful discussions about modeling procedures. The authors also gratefully acknowledge the Molina Center for Energy and the Environment, Gustavo Sosa and the Instituto Mexicano del Petroleo for their help during the MCMA field campaign, Rafael Ramos of RAMA for the use of one of their NO_x instruments. This research is supported by grants from the National Science Foundation (ATM-9984152 and 0612738) and the Camille and Henry Dreyfus Foundation.

Edited by: H. Singh

References

- Baez, A. P., Padilla, H., Garcia, R., Belmont, R., and Torres, M. d. C.: Measurement of indoor-outdoor carbonyls at four residential homes in Mexico City metropolitan area, *Int. J. Environ. Poll.*, 26, 90–105, 2006.
- Bloss, C., Wagner, C., Bonzanini, A., Jenkin, M. E., Wirtz, K., Martin-Reviejo, M., and Pilling, M. J.: Evaluation of detailed aromatic mechanisms (MCMv3 and MCMv3.1) against environmental chamber data, *Atmos. Chem. Phys.*, 5, 623–639, 2005a, <http://www.atmos-chem-phys.net/5/623/2005/>.
- Bloss, C., Wagner, C., Jenkin, M. E., Volkamer, R., Bloss, W. J., Lee, J. D., Heard, D. E., Wirtz, K., Martin-Reviejo, M., Rea, G., Wenger, J. C., and Pilling, M. J.: Development of a detailed chemical mechanism (MCMv3.1) for the atmospheric oxidation of aromatic hydrocarbons, *Atmos. Chem. Phys.*, 5, 641–664, 2005b, <http://www.atmos-chem-phys.net/5/641/2009/>.

- Butler, T. M., Taraborrelli, D., Bruhl, C., Fischer, H., Harder, H., Martinez, M., Williams, J., Lawrence, M. G., and Lelieveld, J.: Improved simulation of isoprene oxidation chemistry with the ECHAM5/MESSy chemistry-climate model: lessons from the GABRIEL airborne field campaign, *Atmos. Chem. Phys.*, 8, 4529–4546, 2008, <http://www.atmos-chem-phys.net/8/4529/2009/>.
- Carr, S., Heard, D. E., and Blitz, M. A.: Comment on “Atmospheric Hydroxyl Radical Production from Electronically Excited NO₂ and H₂O”, *Science*, 324, 336b, doi:10.1126/science.1166669, 2009.
- Colman, J. J., Swanson, A. L., Meinardi, S., Barkley, C. S., Blake, D. R., and Sherwood, R.: Description of the Analysis of a Wide Range of Volatile Organic Compounds in Whole Air Samples Collected during PEM-Tropics A and B, *Anal. Chem.*, 73, 3723–3731, 2001.
- Crowley, J. N. and Carl, S. A.: OH Formation in the Photoexcitation of NO₂ beyond the Dissociation Threshold in the Presence of Water Vapor, *J. Phys. Chem.*, 101, 4178–4184, 1997.
- De Foy, B., Varela, J. R., Molina, L. T., and Molina, M. J.: Rapid ventilation of the Mexico City basin and regional fate of the urban plume, *Atmos. Chem. Phys.*, 6, 2321–2335, 2006, <http://www.atmos-chem-phys.net/6/2321/2009/>.
- Di Carlo, P., Brune, W. H., Martinez, M., Harder, H., Leshner, R., Ren, X., Thornberry, T., Carroll, M. A., Young, V., Shepson, P. B., Riemer, D., Apel, E., and Campbell, C.: Missing OH Reactivity in a Forest: Evidence for Unknown Reactive Biogenic VOCs, *Science*, 304, 722–725, 2004.
- Dunlea, E. J., Herndon, S. C., Nelson, D. D., Volkamer, R. M., Lamb, B. K., Allwine, E. J., Grutter, M., Ramos-Villegas, C. R., Marquez, C., Blanco, S., Cardenas, B., Kolb, C. E., Molina, L. T., and Molina, M. J.: Technical note: Evaluation of standard ultraviolet absorption ozone monitors in a polluted urban environment, *Atmos. Chem. Phys.*, 6, 3161–3180, 2006, <http://www.atmos-chem-phys.net/6/3161/2009/>.
- Dunlea, E. J., Herndon, S. C., Nelson, D. D., Volkamer, R. M., San Martini, F., Sheehy, P. M., Zahniser, M. S., Shorter, J. H., Wormhoudt, J. C., Lamb, B. K., Allwine, E. J., Gaffney, J. S., Marley, N. A., Grutter, M., Marquez, C., Blanco, S., Cardenas, B., Retama, A., Ramos-Villegas, C. R., Kolb, C. E., Molina, L. T., and Molina, M. J.: Evaluation of nitrogen dioxide chemiluminescence monitors in a polluted urban environment, *Atmos. Chem. Phys.*, 7, 2691–2704, 2007, <http://www.atmos-chem-phys.net/7/2691/2009/>.
- Dusanter, S., Vimal, D., and Stevens, P. S.: Technical note: Measuring tropospheric OH and HO₂ by laser-induced fluorescence at low pressure - a comparison of calibration techniques, *Atmos. Chem. Phys.*, 8, 321–340, 2008, <http://www.atmos-chem-phys.net/8/321/2009/>.
- Dusanter, S., Vimal, D., Stevens, P. S., Volkamer, R., and Molina, L. T.: Measurements of OH and HO₂ concentrations during the MCMA-2006 field campaign – Part I: Deployment of the Indiana University laser-induced fluorescence instrument, *Atmos. Chem. Phys.*, 9, 1665–1685, 2009, <http://www.atmos-chem-phys.net/9/1665/2009/>.
- Elshorbany, Y. F., Kurtenbach, R., Wiesen, P., Lissi, E., Rubio, M., Villena, G., Gramsch, E., Rickard, A. R., Pilling, M. J., and Kleffmann, J.: Oxidation capacity of the city air of Santiago, Chile, *Atmos. Chem. Phys.*, 9, 2257–2273, 2009, <http://www.atmos-chem-phys.net/9/2257/2009/>.
- Emmerson, K. M., Carslaw, N., Carpenter, L. J., Heard, D. E., Lee, J. D., and Pilling, M. J.: Urban atmospheric chemistry during the PUMA campaign 1: Comparison of modelled OH and HO₂ concentrations with measurements, *J. Atmos. Chem.*, 52, 143–164, 2005a.
- Emmerson, K. M., Carslaw, N., and Pilling, M. J.: Urban atmospheric chemistry during the PUMA campaign 2: Radical budgets for OH, HO₂ and RO₂, *J. Atmos. Chem.*, 52, 165–183, 2005b.
- Emmerson, K. M., Carslaw, N., Carslaw, D. C., Lee, J. D., McFiggans, G., Bloss, W. J., Gravesstock, T., Heard, D. E., Hopkins, J., Ingham, T., Pilling, M. J., Smith, S. C., Jacob, M., and Monks, P. S.: Free radical modelling studies during the UK TORCH campaign in summer 2003, *Atmos. Chem. Phys.*, 7, 167–181, 2007, <http://www.atmos-chem-phys.net/7/167/2009/>.
- Fortner, E. C., Zheng, J., Zhang, R., Berk Knighton, W., Volkamer, R. M., Sheehy, P., Molina, L., and Andr, M.: Measurements of Volatile Organic Compounds Using Proton Transfer Reaction Mass Spectrometry during the MILAGRO 2006 Campaign, *Atmos. Chem. Phys.*, 9, 467–481, 2009, <http://www.atmos-chem-phys.net/9/467/2009/>.
- George, L. A., Hard, T. M., and O’Brien, R. J.: Measurement of free radicals OH and HO₂ in Los Angeles smog, *J. Geophys. Res.*, 104, 11643–11655, 1999.
- Heard, D. E. and Pilling, M. J.: Measurement of OH and HO₂ in the troposphere, *Chem. Rev.*, 103, 5163–5198, 2003.
- Holland, F., Hofzumahaus, A., Schäfer, J., Kraus, A., and Pätz, H.-W.: Measurements of OH and HO₂ radical concentrations and photolysis frequencies during BERLIOZ, *J. Geophys. Res.*, 108, 8246, doi:10.1029/2001JD001393, 2003.
- Jenkin, M. E., Saunders, S. M., and Pilling, M. J.: The tropospheric degradation of volatile organic compounds: A protocol for mechanism development, *Atmos. Env.*, 31, 81–104, 1997.
- Jenkin, M. E., Saunders, S. M., Wagner, V., and Pilling, M. J.: Protocol for the development of the Master Chemical Mechanism, MCM v3 (Part B): tropospheric degradation of aromatic volatile organic compounds, *Atmos. Chem. Phys.*, 3, 181–193, 2003, <http://www.atmos-chem-phys.net/3/181/2003/>.
- Junkermann, W. and Burger, J. M.: A New Portable Instrument for Continuous Measurement of Formaldehyde in Ambient Air, *J. Atmos. Ocean. Technol.*, 23, 38–45, 2006.
- Kanaya, Y., Cao, R., Akimoto, H., Fukuda, M., Komazaki, Y., Yokouchi, Y., Koike, M., Tanimoto, H., Takegaya, N., and Kondo, Y.: Urban photochemistry in central Tokyo: 1. Observed and modeled OH and HO₂ radical concentrations during the winter and summer 2004, *J. Geophys. Res.*, 112, D21312, doi:10.1029/2007JD008670, 2007.
- Kleffmann, J.: Daytime Sources of Nitrous Acid (HONO) in the Atmospheric Boundary Layer, *Chem. Phys. Chem.*, 8, 1137–1144, 2007, <http://www.atmos-chem-phys.net/8/1137/2009/>.
- Kovacs, T. A., Brune, W. H., Harder, H., Martinez, M., Simpas, J. B., Frost, G. J., Williams, E., Jobson, T., Stroud, C., Young, V., Fried, A., and Wert, B.: Direct measurements of urban OH reactivity during Nashville SOS in summer 1999, *J. Environ. Monit.*, 5, 48–74, 2003.
- Lewis, A. C., Carslaw, D. C., Marriott, P. J., Kinghorn, R. M., Morrison, P., Lee, A. L., Bartle, K. D., and Pilling, M. J.: A larger pool of ozone-forming carbon compounds in urban atmospheres,

- Nature, 405, 778–781, 2000.
- Li, S., Matthews, J., and Sinha, A.: Atmospheric Hydroxyl Radical Production from Electronically Excited NO₂ and H₂O, *Science*, 319, 1657–1660, 2008.
- Madronich, S.: Photodissociation in the atmosphere 1. Actinic flux and the effect of ground reflections and clouds, *J. Geophys. Res.*, 92, 9740–9752, 1989.
- Madronich, S. and Weller, G.: Numerical integration errors in calculated tropospheric photodissociation rate coefficients, *J. Atmos. Chem.*, 10, 289–300, 1990.
- Mao, J., Ren, X., Chen, S., Brune, W. H., Chen, Z., Martinez, M., Harder, H., Lefer, B., Rappengluck, B., Flynn, J., and Leuchner, M.: Atmospheric Oxidation Capacity in the Summer of Houston 2006: Comparison with Summer Measurements in Other Metropolitan Studies, *Atmos. Env.*, doi:10.1016/j.atmosenv.2009.1001.1013, in press, 2009.
- Martinez, M., Harder, H., Kovacs, T. A., Simpas, J. B., Bassis, J., Leshner, R., Brune, W. H., Frost, G. J., Williams, E. J., Stroud, C. A., Jobson, B. T., Roberts, J. M., Hall, S. R., Shetter, R. E., Wert, B., Fried, A., Alicke, B., Stutz, J., Young, V. L., White, A. B., and Zamora, R. J.: OH and HO₂ concentrations, sources, and loss rates during the Southern Oxidants Study in Nashville, Tennessee, summer 1999, *J. Geophys. Res.*, 108, 4617, doi:10.1029/2003JD003551, 2003.
- Merten, A.: New design of Longpath-DOAS instruments based on fibre optics and applications in the study of the urban atmosphere, Thesis, Heidelberg, Univ., Germany, 2008.
- Monks, P. S., Rickard, A. R., and Stacey, L. H.: Attenuation of spectral actinic flux and photolysis frequencies at the surface through homogenous cloud fields, *J. Geophys. Res.*, 109, D17206, doi:10.1029/2003JD004076, 2004.
- Platt, U., Alicke, B., Dubois, R., Geyer, A., Hofzumahaus, A., Holland, F., Martinez, M., Mihelcic, D., Klupfel, T., Lohrmann, B., Patz, W., Perner, D., Rohrer, F., Schafer, J., and Stutz, J.: Free radicals and fast photochemistry during BERLIOZ, *J. Atmos. Chem.*, 42, 359–394, 2002.
- Ren, X., Harder, H., Martinez, M., Leshner, R. L., Oligier, A., Simpas, J. B., Brune, W. H., Schwab, J. J., Demerjian, K. L., He, Y., Zhou, X., and Gao, H.: OH and HO₂ Chemistry in the urban atmosphere of New York City, *Atmos. Environ.*, 37, 3639–3651, 2003.
- Sander, S. P., Friedl, R. R., Golden, D. M., Kurylo, M. J., Moortgat, G. K., Wine, P. H., Ravishankara, A. R., Kolb, C. E., Molina, M. J., Finlayson-Pitts, B. J., Huie, R. E., and Orkin, V. L.: Chemical kinetics and photochemical data for use in atmospheric studies, Evaluation number 15, JPL Publication 06-2, NASA Jet Propulsion Laboratory, Pasadena, California, USA, 2006.
- Saunders, S. M., Jenkin, M. E., Derwent, R. G., and Pilling, M. J.: Protocol for the development of the Master Chemical Mechanism, MCM v3 (Part A): Tropospheric degradation of non-aromatic volatile organic compounds, *Atmos. Chem. Phys.*, 3, 161–180, 2003.
- Sheehy, P., Volkamer, R., Molina, L. T., and Molina, M. J.: Oxidative capacity of the Mexico City atmosphere - Part 2: A RO_x radical cycling perspective, *Atmos. Chem. Phys. Discuss.*, 8, 5359–5412, 2008, <http://www.atmos-chem-phys-discuss.net/8/5359/2009/>.
- Shirley, T. R., Brune, W. H., Ren, X., Mao, J., Leshner, R., Cardenas, B., Volkamer, R., Molina, L. T., Molina, L. T., Lamb, B., Velasco, E., Jobson, T., and Alexander, M.: Atmospheric oxidation in the Mexico City Metropolitan Area (MCMA) during April 2003, *Atmos. Chem. Phys.*, 6, 2753–2765, 2006, <http://www.atmos-chem-phys.net/6/2753/2009/>.
- Sillman, S.: Tropospheric ozone: The debate over control strategies, *Annu. Rev. Energy Environ.*, 18, 31–56, 1993.
- Sinha, V., Crowley, J. N., and Lelieveld, J.: The Comparative Reactivity Method – a new tool to measure total OH Reactivity in ambient air, *Atmos. Chem. Phys.*, 8, 2213–2227, 2008, <http://www.atmos-chem-phys.net/8/2213/2009/>.
- Stockwell, W. R., Kirchner, F., and Kuhn, M.: A new mechanism for regional atmospheric chemistry modeling, *J. Geophys. Res.*, 102, 25847–25879, 1997.
- Velasco, E., Lamb, B., Westberg, H., Allwine, E., Sosa, G., Ariaga-Colina, J. L., Jobson, B. T., Alexander, M. L., Prazeller, P., Knighton, W. B., Rogers, T. M., Grutter, M., Herndon, S. C., Kolb, C. E., Zavala, M., Foy, B. d., Volkamer, R., Molina, L. T., and Molina, M. J.: Distribution, magnitudes, reactivities, ratios and diurnal patterns of volatile organic compounds in the Valley of Mexico during the MCMA 2002 & 2003 field campaigns, *Atmos. Chem. Phys.*, 7, 329–353, 2007, <http://www.atmos-chem-phys.net/7/329/2009/>.
- Volkamer, R., Jimenez, J. L., San Martini, F., Dzepina, K., Zhang, Q., Salcedo, D., Molina, L. T., Worsnop, D. R., and Molina, M. J.: Secondary organic aerosol formation from anthropogenic air pollution: Rapid and higher than expected, *J. Geophys. Res.*, 33, L17811, doi:10.1029/2006GL026899, 2006.
- Volkamer, R., Martini, F. S., Molina, L. T., Salcedo, D., Jimenez, J. L., and Molina, M. J.: A missing sink for gas-phase glyoxal in Mexico City: Formation of secondary organic aerosol, *Geophys. Res. Lett.*, 34, L19807, doi:10.1029/2007GL030752, 2007a.
- Volkamer, R., Sheehy, P. M., Molina, L. T., and Molina, M. J.: Oxidative capacity of the Mexico City atmosphere - Part 1: A radical source perspective, *Atmos. Chem. Phys. Discuss.*, 7, 5365–5412, 2007b, <http://www.atmos-chem-phys-discuss.net/7/5365/2009/>.
- Volkamer, R., Ziemann, P. J., and Molina, M. J.: Secondary Organic Aerosol Formation from Acetylene (C₂H₂): seed effect on SOA yields due to organic photochemistry in the aerosol aqueous phase, *Atmos. Chem. Phys.*, 9, 1907–1928, 2009, <http://www.atmos-chem-phys.net/9/1907/2009/>.
- Wennberg, P. O. and Dabdub, D.: Rethinking Ozone Production, *Science*, 319, 1624–1625, 2008.
- Yoshino, A., Sadanaga, Y., Watanabe, K., Kato, S., Miyakawa, Y., Matsumoto, J., and Kajii, Y.: Measurement of total OH reactivity by laser-induced pump and probe technique – comprehensive observations in the urban atmosphere of Tokyo, *Atmos. Env.*, 40, 7869–7881, 2006.
- Zheng, J., Zhang, R., Fortner, E., Volkamer, R., Molina, L., Aiken, A. C., Jimenez, J. L., Gaeggeler, K., Dommen, J., Dusanter, S., Stevens, P. S., and Tie, X.: Measurements of HNO₃ and N₂O₅ using ion drift-chemical ionization mass spectrometry during the MILAGRO/MCMA-2006 campaign, *Atmos. Chem. Phys.*, 8, 6823–6838, 2008, <http://www.atmos-chem-phys.net/8/6823/2009/>.